*Smart system of renewable energy storage based on **IN**tegrated E**V**s and b**A**tteries to empower mobile, **D**istributed and centralised **E**nergy storage in the distribution grid*

Deliverable nº:	**D6.5**
Deliverable name:	**Advanced battery techno-economics tool**
Version:	**10.**
Release date:	**19/12/2018**
Dissemination level:	**Public**
Status:	**Submitted**
Author:	**Ari Hentunen, Juha Forsström, Victor Mukherjee - VTT**

This project has received funding from the European Union's Horizon 2020 Research and Innovation programme under Grant Agreement No 731148.

Document history:

Version	Date of issue	Content and changes	Edited by
0.1	05/12/2018	First draft version	Ari Hentunen
1.0	19/12/2018	Peer-reviewed and submitted version	Ari Hentunen

Peer reviewed by:

Partner	Reviewer
UPC	Pol Olivella-Rosell
eSmart	Stig Ødegaard Ottesen

Deliverable beneficiaries:

WP / Task
WP5 / Tasks 5.3 & 5.4
WP8 / Tasks 8.3 & 8.5
WP10 / all tasks
WP6 / Task 6.5

Table of contents

Abbreviations and Acronyms

Acronym	Description
AC	Alternating Current
BDF	Benefit-to-Degradation Factor
BMS	Battery Management System
CC	Constant Current
CC-CV	Constant-Current–Constant-Voltage
CV	Constant Voltage
DC	Direct Current
DOD	Depth Of Discharge
DSF	Degradation Stress Factor
DSO	Distribution System Operator
EMS	Energy Management System
EOL	End Of Life
EV	Electric Vehicle
LCOD	Levelized Cost of Degradation
LFP	Lithium Iron Phosphate
LIB	Lithium Ion Battery
LMO	Lithium Manganese Oxide
LNO	Lithium Nickel Oxide
LTO	Lithium Titanate Oxide
MIP	Mixed Integer Programming
NCA	Nickel Cobalt Aluminium
NMC	Nickel Manganese Cobalt
OCV	Open Circuit Voltage
PCS	Power Conversion System
PV	Photovoltaic
RUL	Remaining Useful Life
SCADA	System Control and Data Acquisition
SOC	State of Charge
SOE	State of Energy
SOH	State of Health
SOS2	Special Ordered Sets of type 2

Symbols

Symbol	Description
a	Slope of efficiency curve
b_k	Binary variable
c_j	Marginal cost of degradation at segment *j* [€/MWh]
d_j^{cyc}	Marginal degradation caused by cycle ageing at segment *j* [%]
$e_{t,j}$	Segment energy at time *t* [MWh]
e_j	Segment energy [MWh]
d_j^{cyc}	Segment-wise degradation caused by cycle ageing [%]
i	Interest rate [%]
p_{e}	Grid electricity price [€/MWh]
$p_{t,j}^{\mathrm{ch}}$	Charging power of segment *j* at time *t* [MW]
$p_{t,j}^{\mathrm{dis}}$	Discharging power of segment *j* at time *t* [MW]
q_0	Constant of the linearized function
q	Slope of the linearized function
s_T^{cal}	Coefficient representing the temperature-to-calendar-life stress funtion
w	Tuning coefficient for power constraints
y_k	Value of the *y* coordinate at segment *k* end
B_k	Value of the *x* coordinate at segment *k* end
C_{inv}	Investment cost (or replacement cost) of a battery [€]
C_{deg}	Cost of degradation [€]
C_k	Slope of the linearized curve at segment *k*
D^{cal}	Degradation caused by calendar ageing [%]
D^{cyc}	Degradation caused by cycle ageing [%]
D_0	Planned degradation during the planning period [%]
D_{year}	Planned annual degradation [%]

Symbol	Description
E	Energy capacity of a battery [MWh]
I	Current [A]
I_{spec}	Specified current at which the nominal efficiency is obtained [A]
J	Number of segments
L^{cal}	Calendar lifetime [# years]
L^{cyc}	Cycle lifetime [# cycles]
$L_{\text{ref}}^{\text{cal}}$	Reference calendar life at reference conditions [# years]
$L_{\text{ref}}^{\text{cyc}}$	Reference cycle life at reference conditions [# cycles]
$N_{\text{d-y}}$	Number of days in a year
$N_{\text{h-d}}$	Number of hours in a day
$N_{\text{ts-h}}$	Number of timesteps in an hour
N_{periods}	Number of periods
P_g	Grid power [MW]
$P_{\text{max}}^{\text{ch}}$	Maximum charging power [MW]
$P_t^{\text{ch,ac}}$	Inverter AC charging power at time *t* [MW]
$P_t^{\text{ch,dc}}$	Inverter DC charging power at time *t* [MW]
$P_{\text{max}}^{\text{dis}}$	Maximum discharging power [MW]
$P_t^{\text{dis,ac}}$	Inverter AC discharging power at time *t* [MW]
$P_t^{\text{dis,dc}}$	Inverter DC discharging power at time *t* [MW]
P_t^{ch}	Charging power at time *t* [MW]
P_t^{dis}	Discharging power at time *t* [MW]
R_t	Revenue at time *t* [€]
S_T^{cal}	Temperature-to-calendar-life stress factor
S_ψ^{cal}	State-of-energy-to-calendar-life stress factor
$S_{\psi,\text{lin}}^{\text{cal}}$	Linearized state-of-energy-to-calendar-life stress factor

Symbol	Description
S_T^{cyc}	Temperature-to-cycle-life stress factor
$S_{\psi_{\text{avg}}}^{\text{cyc}}$	Average-state-of-charge-to-cycle-life stress factor
$S_{\Delta\delta}^{\text{cyc}}$	Cycle-depth-to-cycle-life stress factor
T_{life}	Battery lifetime [# years]
T_L	Planned lifetime of a battery [# years]
V_{rev}	Present value of revenues [€]
V_t	Binary variable at time *t*
β_T	Adaptation coefficient during period *T*
φ	Cycle life [# cycles]
φ_N	Normalized cycle life
η	Efficiency [%]
η^{ch}	Efficiency during charging [%]
$\eta_{\text{b}}^{\text{ch}}$	Battery efficiency during charging [%]
η^{dis}	Efficiency during discharging [%]
$\eta_{\text{b}}^{\text{dis}}$	Battery efficiency during discharging [%]
$\eta_{\text{spec}}^{\text{rt}}$	Roundtrip efficiency at a specified rate [%]
ΔD_T	Actual degradation during the planning period *T* [%]
$\Delta\delta$	Cycle depth [% or MWh]
Δt	Time step [h]
Φ	Inverse of cycle life
ψ_t	State of energy at time *t* [%]
$\psi^{\min}$	Minimum state of energy at time *t* [%]
$\psi^{\max}$	Maximum state of energy at time *t* [%]
Ψ_t	State of energy at time *t* [MWh]
$\Psi^{\max}$	Maximum state of energy [MWh]

Symbol	Description
Ψ^{min}	Minimum state of energy [MWh]
ρ	Adaptation coefficient
χ	Calendar lifetime coefficient

Glossary

C-rate	A measure of the rate at which a battery is discharged relative to the manufacturer's rated capacity in ampere-hours. It is also related to the discharge time. For example, if the battery's rated capacity is 40 Ah, then 1C rate is 40 A and the battery is empty after a 1-hour discharge, 2C rate is 80 A and the battery is empty after a 0.5-hour discharge, and C/4 rate is 10 A and the battery is empty after a 4-hour discharge.
Calendar life	The length of time a battery can undergo some defined operation before failing to meet its specified end-of-life criteria.
Capacity	The capacity of a battery expresses the maximum available ampere-hours when a full battery is discharged at a certain C-rate until the cut-off voltage is reached.
Cycle	A sequence of a discharge followed by a charge, or a charge followed by a discharge under specified conditions.
Cycle life	The number of cycles, each to specified discharge and charge termination criteria under a specified charge and discharge regime, that a battery can undergo before failing to meet its specified end-of-life criteria.
Cycle depth	Cycle depth (ΔDOD or ΔSOC) describes the depth of a discharge-charge cycle. Cycle depth is usually expressed in percentage.
Degradation stress factor	Degradation stress factors are all the operation practices or circumstances that accelerate the degradation in battery and thus shorten the lifetime of the cell. Also known as the state of health stress factors.
Depth of discharge	The depth of discharge is a measure of how much charge has been discharged from a full battery. It is usually expressed in percents, but is sometimes expressed also in amperehours.
Discharge rate	See *C-rate*.
E-rate	Similar to *C-rate*, but in terms of power against energy capacity. That is, E-rate describes the rate of discharge power relative to the manufacturer's rated energy capacity in kilowatt-hours. For example, a battery that is discharged at a rate of 1E is fully discharged in an hour.
End of life	The stage at which a battery is not anymore capable to meet its performance criteria regarding capacity or power.
Internal impedance	Opposition to the flow of an alternating current at a particular frequency at a specified state of charge and temperature.
Internal resistance	Opposition to direct current flow in a battery. It is the sum of the ionic and electronic resistances of a battery.

Nominal operating voltage	The average voltage of a battery, as specified by the manufacturer, during discharging at a specified rate and temperature.
Open-circuit voltage	The equilibrium voltage of a battery at a specified state of charge and temperature when there is no current flowing.
Polarization	The voltage deviation from the equilibrium voltage under loading, i.e., when current is flowing.
Self discharge	The process by which the available capacity of a battery decreases spontaneously due to undesirable chemical side reactions or short circuits within a cell.
State of charge	The state of charge is a measure of how much charge is left in a battery. It is a ratio of the present charge and the full charge, and it is usually expressed in percents.
State of energy	The state of energy is a measure of how much energy is left in a battery. It is a ratio of the available stored energy and the nominal energy capacity. It can be expressed in kilowatt-hours and in percents.
State of health	The state of health is a measure of aging. It can be defined for capacity fade and power fade. Typically a battery is considered to be at its end of life when the state of health has decreased to 80%.
Tapering	Tapering refers to the reduction of current and power when the battery approaches fully-charged or fully-discharged state. The high and low cut-off voltages at cell level shall not be exceeded, and hence, the current needs to be reduced when the first cell reaches the cut-off voltage.
Thermal runaway	Thermal runaway occurs in Li-ion batteries when the rate of internal heat generation caused by the exothermic reactions exceeds the rate at which the heat can be expelled. Eventually, the temperature rises rapidly and the battery catches fire and burns at a very high temperature. The fire may catch nearby cells, and eventually, the whole battery may burn down.

Executive summary

This deliverable presents the advanced battery techno-economic model that will be included in the flexibility management allocation and operation algorithm developed in Task 5.4 *Design and program the flexibility management operation algorithm* and described in detail in D5.4 *Advanced battery operation and control algorithm*.

The main objective of this deliverable is to provide a tool that optimizes the battery operation in such a way that maximum economic value can be obtained. Basic technical, economical, and performance characteristics of battery energy storage systems (BESSs) as well as simplified models for the optimization framework were presented in D6.2 *Battery techno-economics tool* [1], which forms the basis for this deliverable. This deliverable adds details and features into the battery modelling methods in general, making it more accurate and usable. Furthermore, the overall optimization problem is now divided into two parts: (i) long-term planning and (ii) short-term operational optimization. With these improvements in the overall methodology and the storage system modelling, higher lifetime benefits can be obtained and the operating conditions impacting the degradation are covered better and in a computationally efficient way.

1 Introduction

This deliverable presents an advanced battery techno-economic model that will be included in the flexibility management allocation and operation algorithm, which is developed in Task 5.4 *Design and program the flexibility management operation algorithm* and described in detail in D5.4 *Advanced battery operation and control algorithm* [2].

The main objective of this deliverable is to provide a tool that optimizes the battery operation in such a way that maximum economic value can be obtained. In order to achieve this, the degradation mechanisms and phenomenons that are affecting the performance need to be identified and characterized. Batteries have very complex ageing characteristics with many stress factors and interdependencies that affect the rate of ageing. These stressors need to be characterized in order to be able to provide limits and constraints for battery operation to ensure long lifetime. This identification and characterization of degradation stress factors (DSFs) is performed in Task 6.2 and reported in D6.3 *Simplified state of health diagnostics tool* [3] and D6.4 *Advanced state of health diagnostics tool* [4]. The main findings of these reports are utilized in this report.

Basic technical, economical, and performance characteristics of battery energy storage systems (BESSs) as well as simplified models for the optimization framework were presented in D6.2 *Battery techno-economics tool* [1], which forms the basis for this deliverable. This deliverable adds details and features into the battery modelling methods in general, making it more accurate and usable. In particular, the modelling of battery degradation now includes also the calendar ageing as a function of the SOE, and both the cycle ageing and the calendar ageing involve another DSFs; temperature. However, the temperature-related DSFs affect indirectly as coefficients representing the impact of the average operating temperature, and therefore, they do not complicate the model much, keeping the model computationally efficient. Furthermore, the overall optimization problem is now divided into two parts: (i) long-term planning and (ii) short-term operational optimization. With these improvements in the overall methodology and the storage system modelling, higher lifetime benefits can be obtained and the operating conditions impacting the degradation are covered better and in a computationally efficient way.

2 Simplified models and advanced models

Battery storage system characteristics and simplified modelling methods were presented in D6.2 [1]. In this Chapter, updates on the storage characteristics and modelling approaches are provided and the differences between the simple models and the advanced models are briefly discussed. The final modelling methodology is presented in Chapters 3 and 4.

2.1 Pilots' storage systems

The pilot sites and applications as well as the technologies and specifications are provided in detail in D10.1 [5]. Generally, the pilots are demonstrating the use of variable energy sources such as photovoltaic (PV) panels as well as controllable loads, such as smart charging of electric vehicles (EVs). The following battery technologies are used in the pilots: (i) lithium nickel manganese oxide (NMC), (ii) a blend of lithium manganese oxide (LMO) and NMC, (iii) lithium iron phosphate (LFP), and (iv) vanadium redox flow battery. A brief summary of the pilot applications and the selected storage technologies are shown in Table 1. All pilots use lithium-ion batteries (LIBs), but the German pilot is demonstrating also the use of a vanadium redox flow technology, which is totally different than lithium ion technologies. The VRFB characteristics of the storage used in the German pilot are described briefly in Section 2.13. The rest of this Chapter deals with lithium-ion technologies.

Table 1: Applications and characteristics of the batteries used in the INVADE pilot sites.

Pilot	Application	Total capacity	Battery type
Bulgaria	Centralized battery for hotel and restaurant, connected to PVs.	201 kWh / 201 kW*	NMC (Samsung SDI)
Norway	30 residential batteries connected to PV systems, EV-chargers and smart heating systems. One battery connected to PV and 11 smart EV-chargers.	30 x 4,2 kWh / 6 kW (residential)	LMO+NMC (AESC Nissan 2nd life) NMC (AESC) LFP (Fronius)
The Netherlands	Centralized battery next to an office building. Power quality and local balancing: solar panels, windmills, EV charging.	138 kWh / 140 kW*	NMC (Samsung SDI)
Spain	Backup battery storage system connected to the grid. Secures electricity supply for critical buildings. Can also be used to balance production and consumption in the area.	211 kWh / 48 kW* (100 kWh for backup, ~100 kWh for balancing)	LFP (ThunderSky-Winston)
Germany	Main value stream: Feed-in of the generation peaks of the PV plants (30 kWp) into the battery system (locally controlled). A second value stream: Peak-shaving of the grid (controlled by the IIP). 10 existing residential batteries connected to PV systems.	120 kWh / 20 kW 2–10 kWh	Vanadium redox flow (Storion) Lithium ion

2.2 Battery efficiency characteristics

A method for evaluating the energy efficiency of a battery at different rates based on the value provided in the specification was presented in D6.2 [1]. It was expected that this method results in conservative values especially at higher rates, because the rate effect and temperature effect are not taken into account in any way. Other influencing factors are the cycle depth and the ambient temperature. An experiment was made to investigate the energy efficiency characteristics of a commercial battery cell in detail. A commercial Kokam 40-Ah NMC battery was tested with a commercial PEC SBT0550 battery tester. The battery was located inside a thermal chamber, which was controlled by the battery tester. The test parameters are gathered in Table 2. The average SOC was 50% for all tests. Therefore, the SOC range of the tests is as follows:

- 100% cycle depth: SOC 100% → 0%
- 50% cycle depth: SOC 75% → 25%
- 10% cycle depth: SOC 55% → 45%

Figure 1–Figure 2 show the test cycle at 25 °C ambient temperature at 100 % cycle depth and 50 % cycle depth, respectively.

Table 2: Test parameters for the efficiency characterization.

Test parameter	Value
Charging voltage	4.15 V
End-of-charge current	C/100
Discharging cut-off voltage	3.20 V
Rest period	2 h
Average SOC	50%
Cycle depths	100%, 50%, 10%
Current rates	C/3, 1C, 2C*
Ambient temperatures	10 °C, 25 °C, 40 °C

* Not applicable at 40 °C ambient temperature.

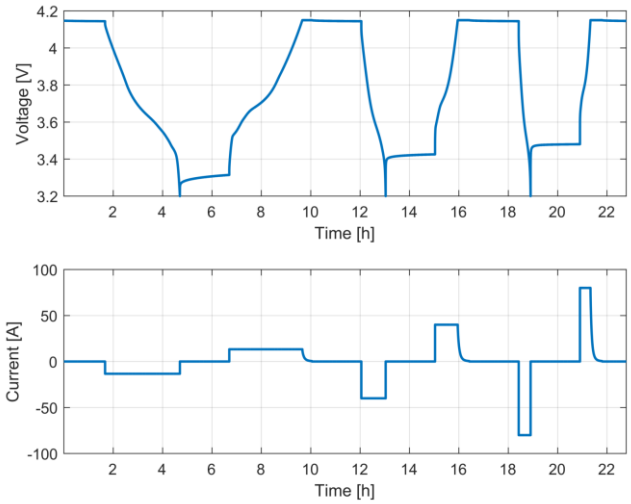

Figure 1: Test cycle at 25 °C ambient temperature and 100 % cycle depth.

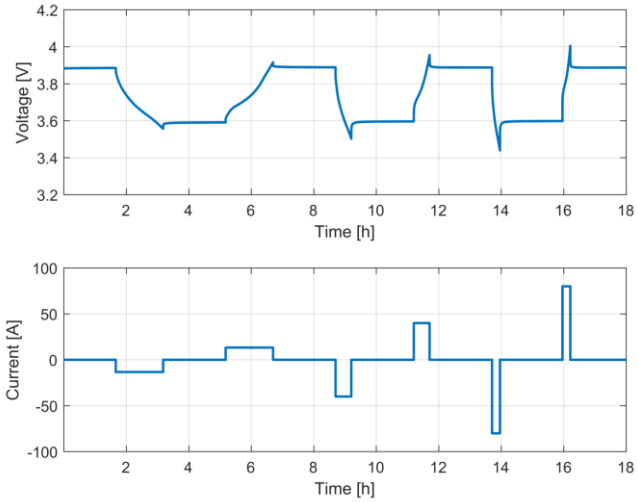

Figure 2: Test cycle at 25 °C ambient temperature and 50 % cycle depth.

Experimental roundtrip energy efficiency at different cycle depths, rates, and ambient temperature are shown in Figure 3. In Figure 4, the experimental results at 25 °C and 100% cycle depth are compared with the analytical results. At higher rates the experimental results were better than the results obtained with the analytical method. Moreover, the efficiency increases slightly at lower cycle depths, which was expected.

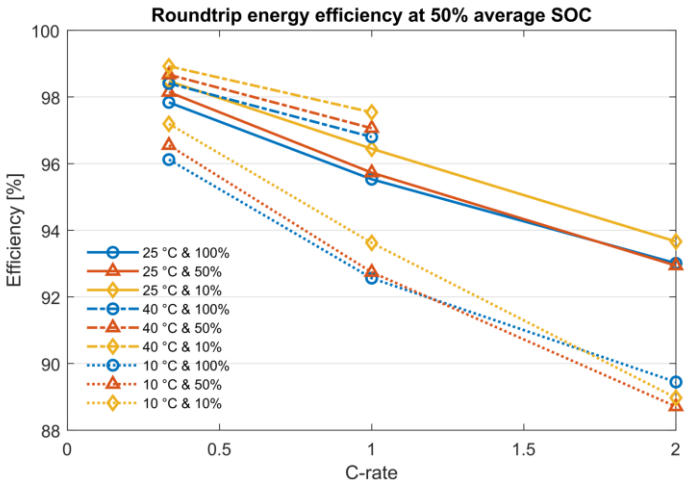

Figure 3: Experimental roundtrip energy efficiency characteristics of a commercial Kokam 40-Ah NMC battery cell.

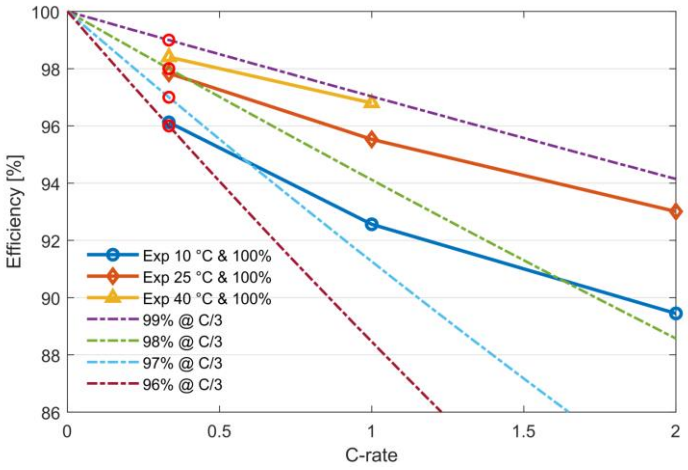

Figure 4: Comparison of the analytical and the experimental results. The analytical curves are defined at the specified roundtrip efficiency and rate, and the curves are calculated based on the analytical model presented in D6.2 [1] and represented in Section 3.5.1.

The results provide evidence that the analytical method gives conservative values at higher rates. Moreover, as the average cycle depth in real applications varies and is always less than 100%, the use of 100% cycle depth in the parameter extraction further increases the conservativeness of the analytical method. However, it must be kept in mind that there are contrary effects as well. First, the cell degradation results in lower efficiency due to increased internal impedance. Second, the lower ambient temperature

results in higher impedance as well, and therefore, in lower efficiency. Moreover, cabling, switches, transformers, etc. cause losses, and therefore, result in lower overall efficiency.

2.3 Storage system efficiency modelling

In the simplified model, a constant efficiency was used for the BESS, i.e., it included the efficiency of the battery and the power conversion system (PCS). However, in order to avoid the low efficiency area of the PCS at low power levels, the nonlinear efficiency characteristics need to be included into the model. The proposed modelling methodology separates the battery efficiency and the PCS efficiency. The battery efficiency is modelled with a constant efficiency, and the nonlinear efficiency of the PCS is characterized with an input–output power mapping with a binary variable or with a special ordered sets of type 2 (SOS2) variable. The SOS2 method is more accurate, but it is also more computationally complex. Moreover, SOS2 is not supported by all solvers, e.g., GLPK does not have a support for the SOS2 variable. Therefore, the input–output mapping with a binary variable can be used in such cases where low computationally burden is required or SOS2 cannot be used.

2.4 Discharging and charging characteristics

Experimental data on constant current (CC) discharging and CC–constant-voltage (CV) charging of the commercial Kokam 40-Ah NMC battery at a rate of 1C at 25 °C ambient temperature is shown in Figure 5. Full voltage region was used in the experiment, i.e., state of charge (SOC) range was 0–100 %. The end-of-constant-voltage (EOCV) charging was C/100, which is a very low rate for practical applications. The boundary between CC and CV charging occurs approximately at 92.5% SOC, after which the current, and consequently, the power are reduced rapidly. As can be seen from the figure, topping up of the battery at CV mode until C/100 rate is slow, as it took 29 min. For C/20 and C/10 rates, the corresponding CV mode duration would be 15 min and 11 min, respectively. If the maximum SOC is limited to 95%, the CV operation lasts only for 2 minutes in this case, which is about the same time as would happen at CC mode. Therefore, a constraint for the maximum SOC shall be set to avoid the slow finishing of the charging. Furthermore, this also prolongs the lifetime of the battery, which is an additional benefit of limiting the voltage range from the top. If the maximum SOC limit would be set so that the CV operation would be avoided at normal operating conditions, i.e., at room temperature and nominal power, there would be no prediction error caused

by the CV operation when operating at nominal operating conditions even without any further power constraints. For the Kokam battery, this would mean that the maximum SOC would be limited to approximately 90 %. This decision would further improve the lifetime of the battery compared to the 95 % limit.

Performance at 10 °C ambient temperature is shown in Figure 6. During discharging, the minimum voltage was hit at approximately 6.5 % SOC. During charging, the CV mode boundary was hit at approximately 85 % SOC, and moreover, it took 57 min to top up the battery at end-of-charging (EOC) rate of C/100. Duration of the CV mode until 95 % SOC was 11 min, which is 5 min more than it would be with CC charging.

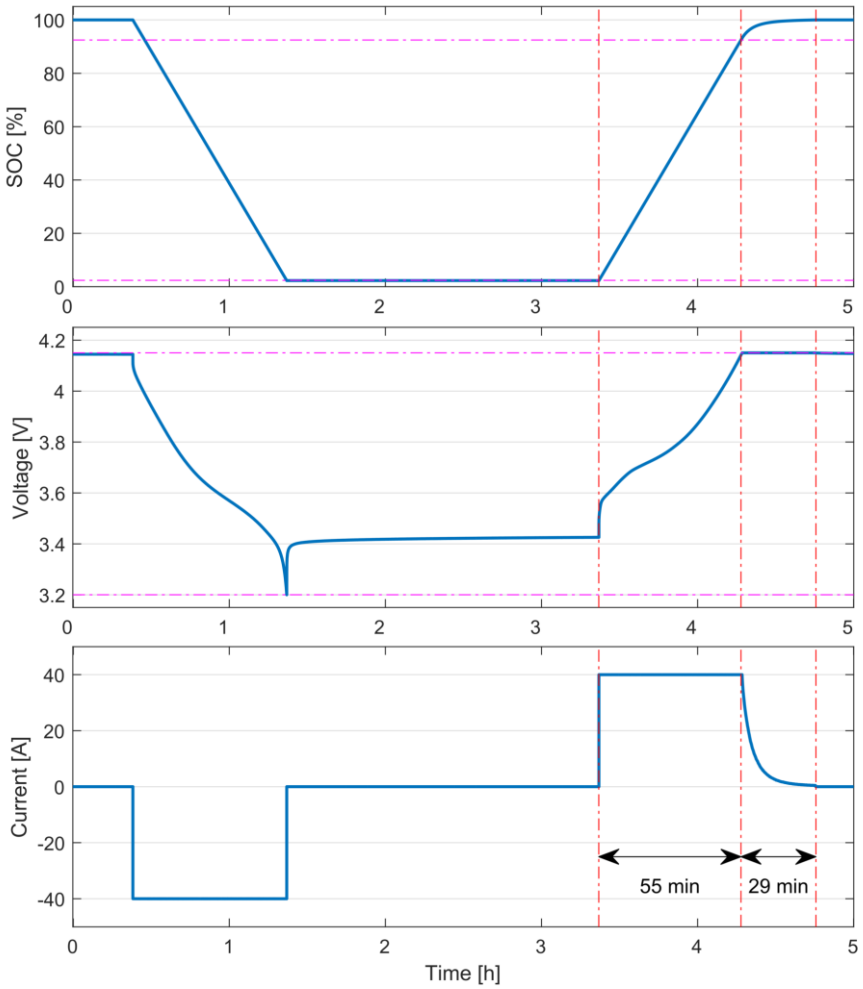

Figure 5: Performance at 25 °C ambient temperature and 1C rate. Constant-current discharge followed by a rest period of 2 h and constant-current–constant-voltage charge. Red vertical lines show the time instants of the boundaries between operating modes during charging.

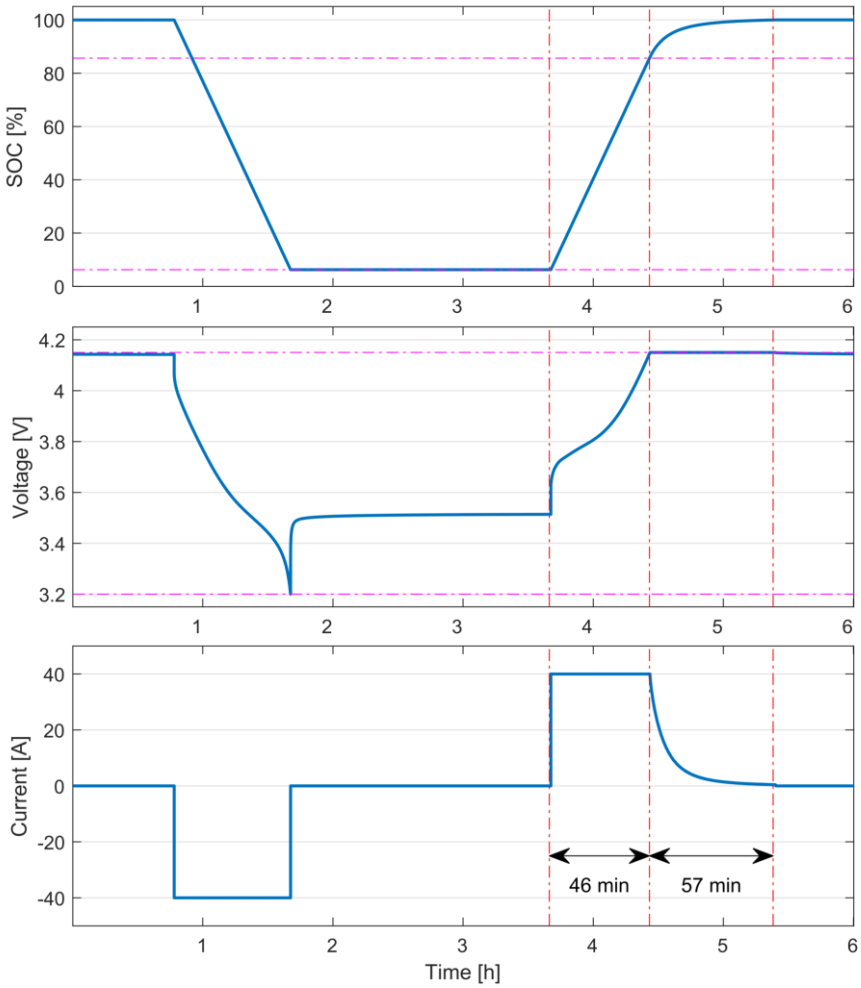

Figure 6: Performance at 10 °C ambient temperature and 1C rate. Constant-current discharge followed by a rest period of 2 h and constant-current–constant-voltage charge. Red vertical lines show the time instants of the boundaries between operating modes during charging.

2.5 State of energy and power constraints

The default minimum and maximum state of energy (SOE) limits of 5 % and 95 %, which were proposed in D6.2, are expected to yield in CC operation in almost full SOE area, when operating in 25 °C or higher ambient temperature. Consequently, only slight prediction error in the SOE is expected to be caused by the occasional CV operation. Furthermore, there is no severe need for additional power constraints. However, if the operating temperature is expected to be commonly below 20 °C, either more narrow SOE window shall be set or additional power constraints shall be used to avoid the minimum and maximum voltages. Practical and computationally efficient implementation of additional power constraints are presented in Section 3.1

2.6 Battery lifetime

Battery degradation characteristics and modelling are described in detail in D6.4 [4]. The main DSFs affecting the cycle life are the cycle depth, the temperature, and the average SOC. The main DSFs affecting the calendar life are the SOC and the temperature [4].

If a battery is cycled repetitively with a specified load profile at a constant ambient temperature, the cycle lifetime L^{cyc} can be estimated as follows:

$$L^{\text{cyc}} = \frac{1}{S^{\text{cyc}}_{\psi_{\text{avg}}}(\psi_{\text{avg}}, \psi_{\text{avg,ref}})} \cdot \frac{1}{S^{\text{cyc}}_{\Delta\delta}(\Delta\delta, \Delta\delta_{\text{ref}})} \cdot \frac{1}{S^{\text{cyc}}_{T}(T_{\text{avg}}, T_{\text{avg,ref}})} \cdot L^{\text{cyc}}_{\text{ref}}, \quad (1)$$

where ψ_{avg} is the average SOE (the midpoint of the cycle), $\Delta\delta$ is the cycle depth, T_{avg} is the average operating temperature, $L^{\text{cyc}}_{\text{ref}}$ is the reference cycle life at reference conditions ($\psi_{\text{avg,ref}}$, $\Delta\delta_{\text{ref}}$, $T_{\text{avg,ref}}$), $S^{\text{cyc}}_{\psi_{\text{avg}}}$ is the average-state-of-charge-to-cycle-life DSF, $S^{\text{cyc}}_{\Delta\delta}$ is the cycle-depth-to-cycle-life DSF, and S^{cyc}_{T} is the temperature-to-cycle-life DSF. At a reference operating point, all DSFs are 1.

Similarly, if a battery is kept at a constant voltage or SOC at a constant ambient temperature, the calendar lifetime L^{cal} expressed in years can be estimated as follows:

$$L^{\text{cal}} = \frac{1}{S^{\text{cal}}_{T}(T_{\text{avg}})} \cdot \frac{1}{S^{\text{cal}}_{\psi}(\psi)} \cdot L^{\text{cal}}_{\text{ref}}, \quad (2)$$

where $N^{\text{cal}}_{\text{n,years}}$ is the reference calendar lifetime in reference conditions expressed in years, S^{cal}_{T} is the temperature-to-calendar-life DSF, S^{cal}_{ψ} is the state-of-energy-to-calendar-life DSF, and $L^{\text{cal}}_{\text{ref}}$ is the reference calendar life at reference conditions.

2.7 Optimal operating area

A summary of the DSFs addressed in the lifetime tests of the reviewed articles in D6.4 [4] is shown in Table 3. Results vary widely depending on the chemistry and even among different studies regarding the same chemistry. The values in the low-stress and optimal-range columns are very coarse generalisations based on the results.

Table 3: Summary of the degradation stress factors addressed in the lifetime tests of the reviewed articles in [4].

Stressor	High stress	Low stress	Optimal range
Cycle depth (ΔDOD)	High ΔDOD	< 50%	< 30%
Temperature	High and low temperature	10–35 ˚C	15–30 ˚C
Current (C-rate)	High rate	< 1C	< C/2
SOC / voltage	High SOC / voltage	< 4 V	< 70% SOC

The operational decisions are based on the flexibility management algorithm, and hence, this algorithm dictates indirectly the average cycle depth, C-rate, and SOC of the battery. Consequently, the typical operating area can be controlled by modelling these stress factors and including their effect on the degradation into the objective function. However, the modelling of the stressors increases the computational complexity of the model significantly, and therefore, only the stressors that have the highest impact shall be included in the optimization. Moreover, simplified approaches shall be developed to decrease the computational burden.

2.8 State of health

The state of health (SOH) of a battery is not estimated within the integrated INVADE platform (IIP). However, the SOH indication will be obtained either from the energy management system (EMS) or by applying regularly a SOH diagnostics tool, which is described in detail in D6.4 [4]. This SOH diagnostics tool is an offline toolkit that can be run locally at the pilot site. It uses the battery usage data provided by the IIP or the supervisory control and data acquisition (SCADA) system and provides an estimate of the remaining capacity of the battery as an output. This capacity estimate is then updated to the IIP by the IIP operator.

2.9 Degradation modelling

The simplified model included only the cycle depth stressor, whereas the advanced model includes also the SOC and the temperature stressors. The operating temperature data is not collected in the IIP, and hence, actual temperature data cannot be used in the optimization. However, this was not intended in the first place, as it would further

complicate the model. Instead, the selected approach is to use historical long-term average temperature from the local SCADA system, which can be updated regularly by the IIP operator. In this way, the long-term average temperature is used to calibrate the degradation rate of the battery. If the temperature data is not available in the SCADA system, the parameter shall be set to resemble the average ambient temperature or the expected average operational temperature of the battery.

2.10 Separation into planning problem and operational problem

In D6.2 [1], the operational optimization algorithm included the levelized cost of degradation (LCOD) in the objective function to address the costs that are related to the battery degradation. The LCOD was obtained by calculating the marginal degradation caused by cycling and by utilizing either the investment cost or the replacement battery cost. The cycle depth stress factor was incorporated into the algorithm by applying the equivalent rainflow counting algorithm proposed by Xu et al. in [6]. This approach has three drawbacks: (i) The future benefits are not discounted, (ii) the battery lifetime and the replacement battery cost are not known initially, and (iii) the operational decisions are solely based on the technical and economical parameters, and therefore, the battery may be totally unused or overused in some cases. For example, a battery with high investment cost or low cycle lifetime may be used very little in cases where the benefits are low. However, even in that case, it is not meaningful not to use the battery at all, because the investment has already been made, and the battery has a limited calendar life as well. Therefore, it would be better to use the battery to obtain the available benefits to minimize the losses.

In a recent article [7], He et al. proposed an intertemporal decision framework for the management of a storage, in which the optimal usage of the storage in the economic sense is first planned for the long term, which is followed by the formulation of the operational decision-making in the short term. The operational algorithm includes the battery degradation in the objective function, but it excludes the investment cost of the battery, because the investment cost is a sunken cost that should not affect the operational decision making. This approach is intuitive and solves the main problems of the LCOD method. However, it requires additional efforts to first determine the optimal usage and later on to manage the utilization of the battery and the associated rate of degradation according to the predefined plan.

The idea of separating the main problem into long-term planning problem and short-term operational problem was adopted in this deliverable. A comprehensive methodology that covers both problems is described in detail in Chapter 3.

2.11 End of life

End of life of a battery is when it no longer meets its performance requirements. As long as safety is maintained, the limit of performance requirements can be decided internally, but normally end of life (EOL) is when the performance is about 60–80 % of its rated performance.

In order to identify when the EOL of a battery is reached, the SOH of the battery needs to be tracked. Many battery management systems (BMSs) and EMSs provide some SOH indication, which can be based simply on coulomb-counting or on more advanced methods. In INVADE, a SOH diagnostics tool was developed in T6.4. The tool is an Excel-based offline tool that can be used locally by the pilots. The tool incorporates a detailed battery degradation model that addresses the degradation stress factors to the historical usage data of the battery system. Time-series data is given as an input, and the estimated SOH is provided as an output. The IIP operator can then update the battery capacity parameter to the IIP. It is suggested to update the parameters on a monthly basis.

The EOL is highly dependent on the application-specific performance requirements and the techno-economics of the use case. At some point, a critical performance requirement cannot be anymore achieved, or the flexibility profit no longer exceeds the marginal cost of operation. A default EOL criterion of 70 % of the original capacity (i.e., 70 % SOH) will be used for INVADE pilot batteries, but it can be adapted for each pilot based on the application-specific requirements, battery technical specification and warranty terms and conditions, and techno-economic evaluations.

2.12 Second-life batteries

From the modelling point-of-view, second-life batteries will be considered as normal batteries. The degraded performance characteristics are reflected in the battery model parameters. Generally, the efficiency is typically lower due to increased impedance. This has also implications to the power constraints, because the voltage limits are hit sooner than for new batteries. Therefore, it may be appropriate to use more conservative

minimum and maximum SOE limits or, alternatively, to implement additional power constraints.

2.13 Vanadium redox flow battery

Redox flow batteries (RFBs) are different from conventional batteries in that they use two electrolytes as energy carriers which are located in external tanks and pumped through a stack of electrochemical cells. The electrolytes are divided by using a separator, e.g., an ion-selective membrane, which allows selected ions to pass and complete the chemical reaction during charging and discharging. In RFBs the energy capacity and power capacity can be decoupled: the energy capacity is dictated by the volumes of active materials, while the power capability is determined by the membrane surface area.

Redox flow batteries do not suffer from processes that lead to mechanical degradation of the active material or formation of dendrites. Therefore, their cycle lifetime is very long and there is no danger of internal shortcircuiting caused by the dendrites. The vanadium RFB is the most commercially developed flow battery [8]. Its cycle life is affected mainly by the stability of the membrane in the highly corrosive V(V) solution in the charged positive half-cell electrolyte [8]. Membranes with up to 10 years have been developed, allowing 10-years of operation before replacement of the membrane. A BMS is also needed to ensure that no extended overcharge occurs that could damage the positive electrode. Cycle life values of over 200,000 cycles have been reported in large systems [9].

The efficiency of vanadium redox flow batteries (VRFBs) is significantly lower than that of LIBs. The coulombic efficiency of VRFBs is affected by two factors: (i) side reactions such as gassing during charging, and (ii) self-discharge caused by the diffusion of vanadium ions across the membrane. Also ohmic losses and polarization losses occur in the cell during loading, which reduce the energy efficiency. Moreover, additional polarization losses occur at high and low SOC, which is why most VRFBs are used within 10–90 % SOC range [8]. Maximum overall energy efficiency of approximately 80 % has been demonstrated [9].

For battery modelling in the INVADE project, the degradation stress factors shall not be used for VRFBs, i.e., all DSFs shall be set to 1 for all input values. Another exception is that the default value for the efficiency shall not be used in any case. Instead, the battery efficiency shall be determined from the technical specification or requested from the battery system provider.

3 Short-term optimization

3.1 Battery storage system model

The SOE is dictated by the cumulative net energy of the battery, i.e, the difference between the charged and discharged energy, and it needs to stay within the specified minimum ($\Psi_{\min}$) and maximum ($\Psi_{\max}$) limits:

$$\Psi_t = \Psi_{t-1} + \Delta t \left[P_t^{\mathrm{ch}} \cdot \eta^{\mathrm{ch}} - \frac{P_t^{\mathrm{dis}}}{\eta^{\mathrm{dis}}} \right] \tag{3}$$

$$\Psi^{\min} \le \Psi_t \le \Psi^{\max} \tag{4}$$

$$\psi_t = \frac{\Psi_t}{E_{\mathrm{n}}} \tag{5}$$

where Ψ is the SOE, Δt is the time step, P_t^{ch} is the charging power, P_t^{dch} is the discharging power, η^{ch} is the total ESS efficiency during charging, η^{dch} is the total ESS efficiency during discharging, and ψ is the SOE expressed in per unit values.

Upper bounds for charging and discharging power are defined as

$$\begin{aligned} P_t^{\mathrm{dis}} &\le V_t P_{\max}^{\mathrm{dis}} \\ P_t^{\mathrm{ch}} &\le \left(1 - V_t\right) P_{\max}^{\mathrm{ch}} \end{aligned} \tag{6}$$

where P^{ch} and P^{dch} are the power constraints regarding charging and discharging, respectively, and the variable *V*(*t*) is a binary variable which ensures that charging and discharging cannot take place during the same time step.

Constant energy capacity shall be used in the model. That is, the rate effect and the temperature effect to the capacity will not be taken into account. However, the energy capacity parameter will be updated regularly by the IIP operator to take into account the battery degradation due to ageing.

The use of equivalent rainflow counting algorithm for online calculation of the marginal degradation caused by the cycle depth stress factor was proposed in D6.2 [1]. In order to implement the equivalent rainflow algorithm, the battery needs to be divided into equal-sized segments. This will be presented next. The following notation is used: small letters

are used for segments, *J* is the number of equally sized segments, subscript *j* denotes segment *j*, and *e* is used for segment-wise energy.

Segment energy balances:

$$e_{t,j} - e_{t-1,j} = \Delta t \left(\eta^{\text{ch}} p_{t,j}^{\text{ch}} - \frac{1}{\eta^{\text{dis}}} p_{t,j}^{\text{dis}} \right) \tag{7}$$

Segment energy bounds:

$$\begin{aligned} e_{1,j} &= e_j^0 \\ e_{t,j} &\le e_j^{\max} \end{aligned} \tag{8}$$

Constraints relating segment energies and the battery energy:

$$\Psi^{\min} \le \sum_{j=1}^{J} e_{t,j} \le \Psi^{\max} \tag{9}$$

$$\sum_{j=1}^{J} e_{t,j} \ge \Psi^{\text{final}} \tag{10}$$

Constraints on charging and discharging power:

$$\begin{aligned} P_t^{\text{dis}} &= \sum_{j=1}^{J} p_{t,j}^{\text{dis}} \\ P_t^{\text{ch}} &= \sum_{j=1}^{J} p_{t,j}^{\text{ch}} \end{aligned} \tag{11}$$

$$\begin{aligned} P_t^{\text{dis}} &\le P_{\max}^{\text{dis}} \cdot V_t \\ P_t^{\text{ch}} &\le P_{\max}^{\text{ch}} \cdot (1 - V_t) \end{aligned} \tag{12}$$

3.2 Additional charging and discharging constraints

Additional power constraints to avoid reaching maximum and minimum voltages, where current needs to be limited, can be defined as follows:

$$P_t^{\text{dis}} \le \frac{\left[\psi_{t-1} - \psi^{\min} \right]}{(1+w)\Delta t} \cdot P_{\max}^{\text{dis}} \tag{13}$$

$$P_t^{\text{ch}} \le \frac{\left[\psi^{\max} - \psi_{t-1} \right]}{(1+w)\Delta t} \cdot P_{\max}^{\text{ch}}, \tag{14}$$

where Δt is the time step in hours and w is a tuning coefficient, which can be different for charging and discharging. $w = 0$ is the implicit constraint, while $w > 0$ reduces the

power. The power constraints are illustrated in Figure 7 and Figure 8, in which $w = 0.2$ was used.

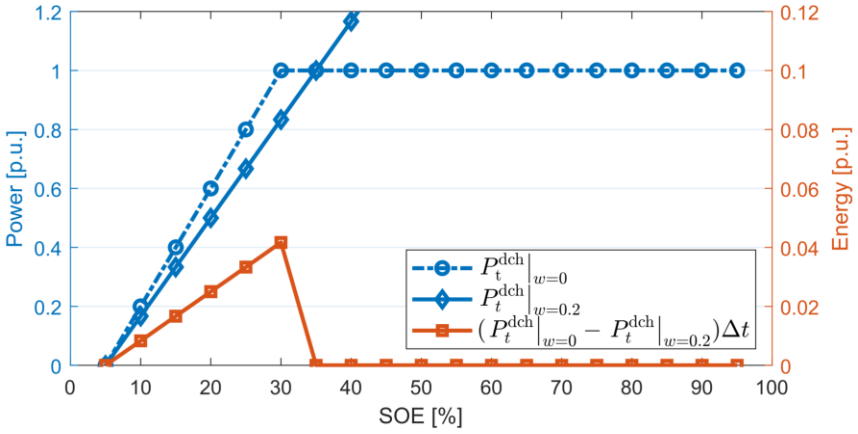

Figure 7: Discharging power constraint. The blue dashed line describes the maximum power to reach the 5 % minimum SOE during one time step, i.e., $w = 0$. The blue solid line describes the reduced discharge power and the red solid line (right axis) shows the energy left in the storage above the minimum level due to the applied power constraint.

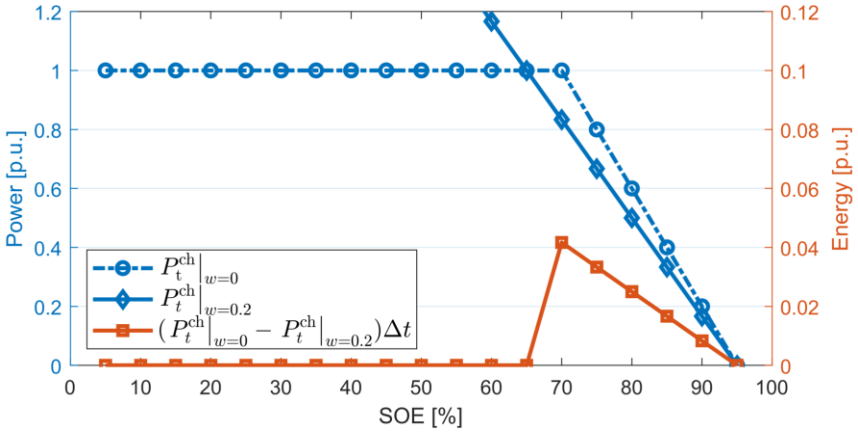

Figure 8: Charging power constraint. The blue dashed line describes the maximum power to reach the 95 % maximum SOE during one time step. The blue solid line describes the reduced charging power and the red solid line shows the energy left in the storage below the maximum level due to the applied power constraint.

3.3 Efficiency

3.3.1 Introduction

The efficiency of the PCS is highly nonlinear at low power regime. Advanced methods to model the efficiency characteristics are described in this Section. The main idea is to separate the efficiency into two parts: (i) the battery system and (ii) the PCS. A constant efficiency is used for the battery system, but the PCS is represented as an input–output

mapping regarding power. The mapping is defined as a piecewise linear function. The efficiency characteristics are embedded into this mapping.

Figure 9 shows the system under study. Equations for the inverter on the discharging side and charging side are presented in (15) and (16), respectively, where $P_t^{\text{dis,ac}}$ is the inverter alternating current (AC) discharging power at time *t*, $P_t^{\text{dis,dc}}$ is the inverter direct current (DC) discharging power, η^{inv} is the inverter efficiency, $P_t^{\text{ch,ac}}$ is the inverter AC charging power, $P_t^{\text{ch,dc}}$ is the inverter DC charging power. These inverter efficiencies are inherently nonlinear functions of power. The implementation of the nonlinear efficiency characteristics is presented next.

$$P_t^{\text{dis,ac}} = \eta^{\text{inv}}(P_t^{\text{dis,dc}}) \cdot P_t^{\text{dis,dc}} \tag{15}$$

$$P_t^{\text{ch,dc}} = \eta^{\text{inv}}(P_t^{\text{ch,ac}}) \cdot P_t^{\text{ch,ac}} \tag{16}$$

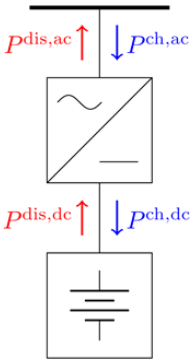

Figure 9: Battery storage system.

3.3.2 Implementation issues

Two implementations, which are based either on SOS2 variables or on applying binary variables directly, are presented. The final decision on the method depends on the requirements regarding the computational complexity and the capabilities of the solver. The binary variable method is suitable for all solvers, whereas the SOS2 variables are not supported e.g. by the GLPK solver.

The inverter efficiency characteristics and the corresponding input–output mapping are shown in Figure 10. Although not clearly visible on the right panel, the slope of the first 10 % of the range is different from the rest. By dividing the input range in two parts we end up having a two-segment model in which the segments are defined by the input power level. The first segment describes the first 10 % of the input power range, [0,0.1],

and the second [0.1,1.0]. Therefore, the relation of the input and the output power consists of two lines: The first covers input power from 0 to 0.1 and the second from 0.1 to 1. The two segment model is a feasible compromise between accuracy and model complexity.

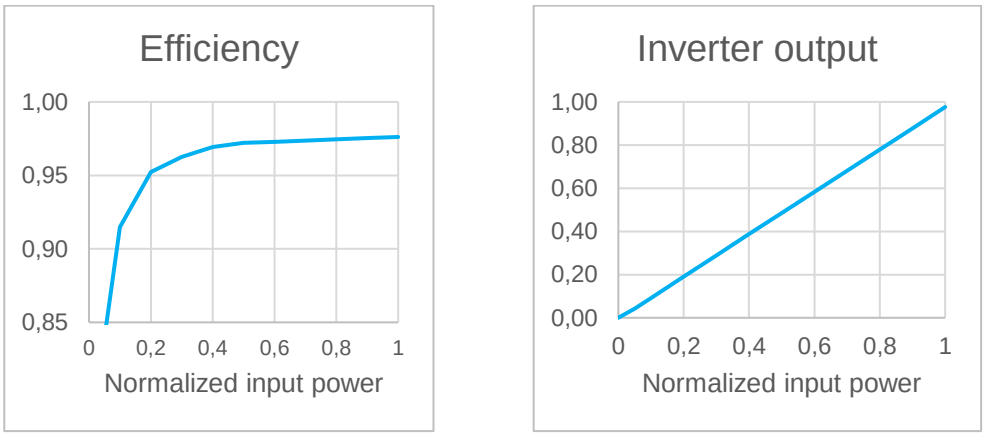

*Figure 10: Inverter efficiency (left panel) and its output (efficiency*input power) (right panel).*

Connecting two interacting segments to describe one piece of equipment calls for a specific approach. Figure 11 explains the approach. The improvement in efficiency decreases incrementally: $C_1>C_2>C_3$.

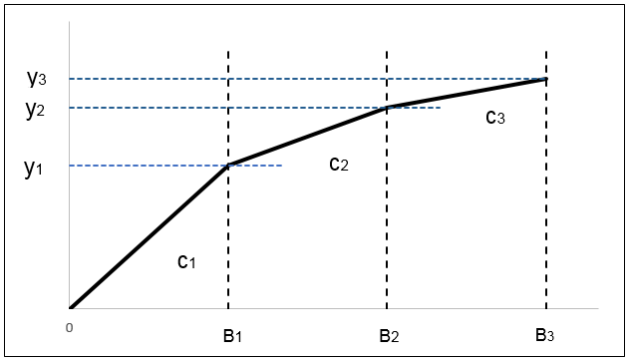

Figure 11: Incremental efficiency breaks.

3.3.2.1 SOS2 method

Referring to Figure 11, we introduce decision variables w_i at the points 0, B1, B2 and B3. In addition, we define *y* axis values that correspond to the total output (*y*) of the inverter using a certain input power level 0, B1, B2, B3:

$$\begin{aligned} y_0 &= 0 \\ y_1 &= C_1 \cdot B_1 \\ y_2 &= y_1 + C_2 \cdot (B_2 - B_1) \\ y_3 &= y_2 + C_3 \cdot (B_3 - B_2). \end{aligned} \tag{17}$$

Then we can write

$$\begin{aligned} \sum_i w_i &= 1 \\ \sum y_i \cdot w_i &= P^{\text{out}} \\ \sum_i B_i \cdot w_i &= x, \end{aligned} \tag{18}$$

where $w_i \in SOS2$ (Special Order Sets of type 2). SOS2 means that at most two of the w_i can be non-zero, and if there are two non-zeros, they must be contiguous: They are the end points of the line segment. The algorithm interpolates linearly between these points to find an exact output relating to the input.

3.3.2.2 Binary variables method

Referring to Figure 11, it is possible to define the problem using binary variables, b_i, for the same problem. The decision variable x (input power) describes the activity in each cost segment. The total activity is

$$x = \sum_i x_i \tag{19}$$

In this method the starting point is always the origin and the search proceeds to the right so far that the equation (19) is fulfilled. The following set of constraints describes this process in which the order is strictly defined:

$$\begin{gathered} B_1 \cdot b_2 \le x_1 \le B_1 \cdot b_1 \\ \left(B_2 - B_1\right) \cdot b_3 \le x_2 \le \left(B_2 - B_1\right) \cdot b_2 \\ x_3 \le \left(B_3 - B_2 \cdot\right) \cdot b_3 \end{gathered} \tag{20}$$

A general definition of the constraints on decision variables:

$$\left(B_i - B_{i-1}\right) \cdot b_{i+1} \le x_i \le \left(B_i - B_{i-1}\right) \cdot b_i \tag{21}$$

And for the binary variables we define

$$b_1 \ge b_2 \ge b_3 \tag{22}$$

This last constraint ensures that the y_i values of (17) will be calculated the same way in this approach as in the SOS2 case. The total output power of the inverter is obtained by summing up all the segments:

$$P^{\text{out}} = \sum_i C_i \cdot x_i \tag{23}$$

Notice that we cannot operate in efficiency area 3 without first activating the first two segments.

Now we are ready to apply the binary variable approach to the inverter description using the sa data in Figure 10. Notice that we do not make a piecewise linear description of the efficiency curve. Instead, we define a piecewise linear model of the inverter output as a function of the input.

The first segment covers the input power range [0,0.1] and the second [0.1,1]. At input power level P_{in}=0, the inverter output, P_{out}, is zero and at P_{in}=0.1, the inverter output is 0.0915. The second segment defined by its end points, [P_{in},P_{out}], are the following: [0.1, 0.0915] and [1.0, 0.976]. The slopes of the line segments describing the inverter are: C_1=0.915, C_2=(0.976-0.0915)/(1-0.1)=0.983.

These values are not efficiencies but coefficients relating input to output. The output of the inverter is obtained by summing up all the segments, as shown in (23). The efficiency is obtained by dividing the total output with the total input.

The binary variable approach took less time than the SOS2 method in the test environment used (GAMS, CPLEX). Although the methods are equivalent in principle, the actual implementations and the many coefficients that control the solver performance lead in practice to similar but not equivalent solutions.

3.3.2.3 Comparison

The binary variable method and the SOS2 variable method are compared in Figure 12. It is evident that SOS2 approach leads to a slightly larger variability in the SOE values compared to that of the binary variable. However, the difference in the minimum total electricity purchase cost was only 0.1 %, i.e., negligible.

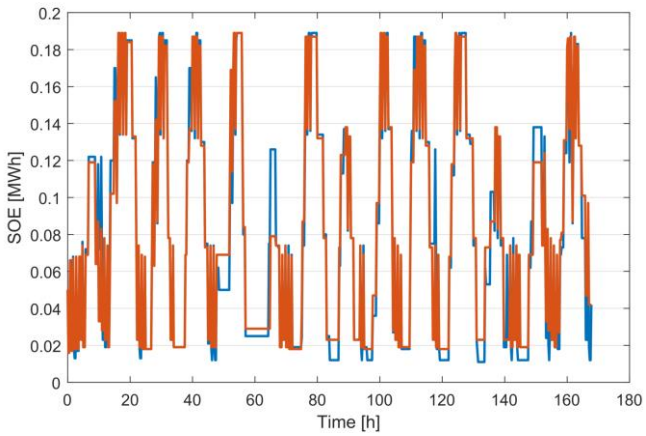

Figure 12: Comparison of SOE development in a test case using CPLEX solver.

3.4 Battery degradation

The advanced battery degradation model includes the following parts:

- Cycle ageing as a function of the cycle depth
- Calendar ageing as a function of the SOE

The cycle depth is considered as the most important DSF, because it has a significant impact on the lifetime of the battery, and importantly, it can be directly controlled by the operational algorithm. The calendar ageing was included to provide more realistic degradation characteristics, and hence, more accurate estimate of the cost of degradation. Because of the calendar ageing, the degradation happens even without using the battery at all. With the cost of degradation involved in any case, it becomes clear that the battery shall be used at least for some extent even in such cases where the real cost of degradation is always higher than the available benefits. As the calendar ageing is a function of the SOC, the optimization results in operating the battery mostly in the operating area that maximizes the calendar life.

In addition to the above-mentioned DSFs, the temperature-related stress factors regarding the cycle ageing and the calendar ageing are included indirectly through coefficients. However, due to lack of battery operating temperature data in the IIP, an estimate of the average operating temperature must be used. This parameter is set by the IIP operator based on either an estimate or the actual historical data from the SCADA system or the BMS. Average operating temperature based on historical data shall be used. Therefore, the long-time effect of the temperature stress factor is taken into account in the degradation, but the optimization algorithm is not burdened computationally by it.

3.4.1 Degradation stress factors

The DSF characteristics are addressed in detail in D6.4 [4]. In general, each battery type has unique DSF characteristics. Therefore, in order to obtain accurate and reliable DSF characteristics, they should be requested from the battery integrator or they should be characterized experimentally. Unfortunately, the battery manufacturers or the battery system integrators are often not willing to provide these characteristics to the customers, and it is very time consuming to extract them experimentally. Therefore, data and models from the literature are often used to estimate the DSFs. The disadvantage of this approach is that these models do not represent the actual battery type in the application, and therefore, high uncertainty is introduced in the model reliability. The big trends in the

DSF characteristics are certain and proven in the scientific literature, but the uncertainty is related to the detailed shape of the curves and especially to the level of the values far away from the nominal point. Example DSF characteristics are shown in Figure 13–Figure 16. The normalized lifetime is shown always in the left axis and the stress factor in the right axis, respectively.

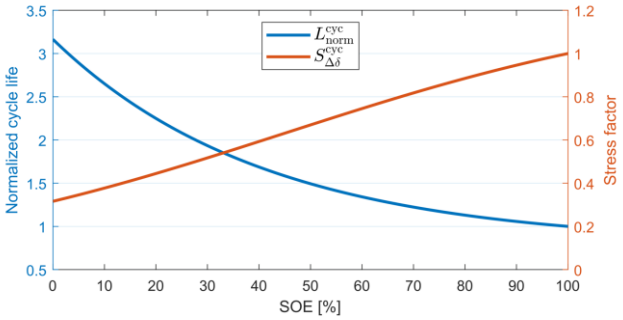

Figure 13: Example of the cycle-depth-to-cycle-life stress factor characteristics. The cycle life data is normalized to 100% SOE, which corresponds to unity stress factor.

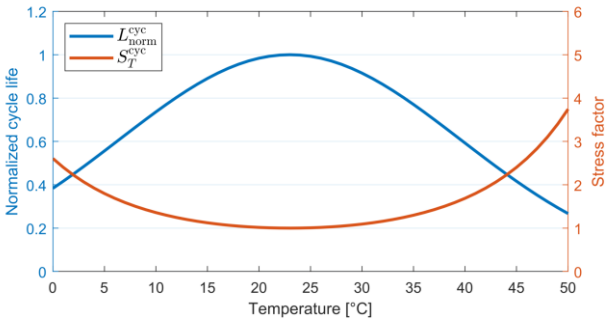

Figure 14: Example of the temperature-to-cycle-life stress factor characteristics.

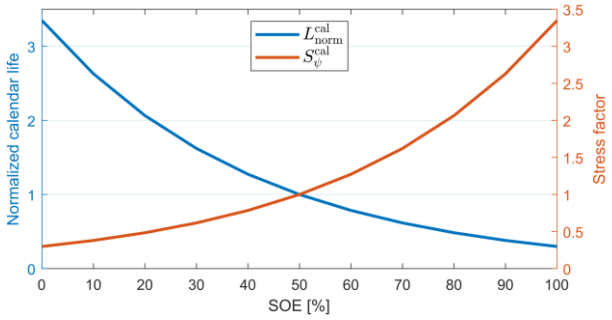

Figure 15: Example of the state-of-energy-to-calendar-life stress factor characteristics. The calendar life data is normalized to 50 % SOE, which corresponds to unity stress factor.

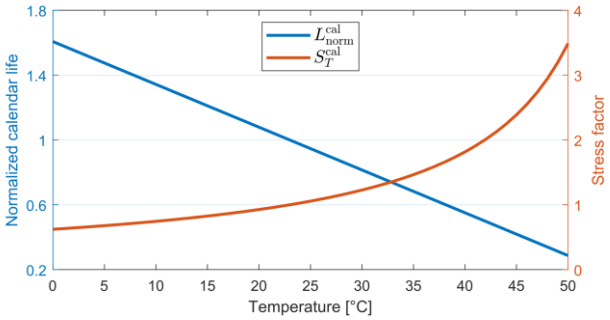

Figure 16: Example of the temperature-to-calendar-life stress factor characteristics. The calendar life data is normalized to 23 °C temperature, which corresponds to unity stress factor.

The lifetime models of (1)–(2) cannot be used in the optimization framework. Instead, we need to calculate the degradation at each time step. The total degradation D is calculated by summing the degradation caused by cycle ageing and calendar ageing, D^{cyc} and D^{cal}, respectively, as shown in (24). In literature, the degradation is typically defined as the lost capacity with respect to the nominal capacity. However, in the modelling part of this report, the degradation is defined as the lost capacity with respect to the anticipated lifetime in the application, i.e., the cycle lifetime and calendar lifetime until the EOL criterion has been reached. Therefore, the range of the value is from 0 to 1, or equivalently, from 0–100 %, with 100 % meaning that the battery capacity has reached the EOL criterion[1].

$$D = D^{\text{cyc}} + D^{\text{cal}} \tag{24}$$

3.4.2 Degradation caused by cycle ageing

The cycle depth at each time step cannot be directly determined during the operation. Therefore, an equivalent rainflow counting algorithm [6] is applied to determine the half cycles and full cycles during the operation, and consequently, to determine the associated marginal degradation. The implementation and application of the equivalent rainflow counting algorithm was discussed in detail in [1]. We start here by defining some concepts of battery use, and based on these concepts, we derive the degradation equations to be used in the optimization algorithm.

In the equivalent rainflow algorithm, the battery is divided into *J* equally-sized segments having an energy capacity of e_j. Generally, both the accuracy and the computational complexity increase with increasing *J*. It was demonstrated in [6] that 10 segments

[1] Typical EOL criterion is 70 % of the nominal capacity.

provide good accuracy and that the improvements in the accuracy become negligible after 16 segments. All simulations in this report have been performed by using ten segments.

One of the basic concepts is the cycle depth, which is the difference of the DOD at the beginning and the end of the discharge or charge half cycle. We define it both for each segment ($\Delta\delta_j$) and for the battery as a whole ($\Delta\delta$).

Cycle depth at segment level:

$$\Delta\delta_{t,j} = \frac{e_{t,j} - e_{t-1,j}}{E} = \frac{\Delta e_{t,j}}{E} = \frac{\Delta t \cdot P_{t,j}^{\text{dis}}}{E}, \tag{25}$$

where *E* is the energy capacity of the battery. Using segment and battery capacities we define the cycle depth of one segment as follows:

$$\Delta\delta_j = \frac{e_j}{E} = \frac{1}{J}. \tag{26}$$

This constant value applies for all segments.

Cycle depth at battery level is obtained by summing up over all the segments:

$$\Delta\delta_t = \frac{\sum_j \Delta e_{t,j}^{\text{dis}}}{E}. \tag{27}$$

Battery lifetime is usually described as the number on normalized cycles. The equation that relates the normalized cycle life φ_N to actual cycles φ and cycle depth is as follows:

$$\varphi_N = \frac{\varphi(\Delta\delta)\cdot\Delta\delta}{\varphi_{100}}, \tag{28}$$

where φ_{100} is the number of cycles of 100 % cycle depth. The life loss function (degradation) is defined as an inverse of the cycle-depth dependent number of cycles, as follows:

$$D^{\text{cyc}} = \frac{S_{\Delta\delta}^{\text{cyc}}(\Delta\delta)}{L_{\text{ref}}^{\text{cyc}}} = \Phi(\Delta\delta) = \frac{1}{\varphi(\Delta\delta)} \tag{29}$$

Degradation is defined above for the whole battery, but we are interested in defining it separately for each segment and summing them up to get the total degradation. Therefore, the marginal degradation as a function of discharge in each segment is defined as follows:

$$d_j^{\mathrm{cyc}} = \frac{\Delta\Phi\left(\Delta\delta_j\right)}{\Delta\delta_j} = \frac{\Phi(j)-\Phi(j-1)}{\frac{e_j}{E}} = \frac{E}{e_j}\cdot\Delta\Phi_j . \tag{30}$$

At each time step, the battery degradation can now be defined on the basis of per segment discharged energy:

$$D_t^{\mathrm{cyc}}(\Delta\delta_t) = \sum_j d_j^{\mathrm{cyc}} \cdot \left(\frac{\Delta e_{t,j}^{\mathrm{dis}}}{E}\right) = \sum_j \left[\Delta\Phi_j \cdot \frac{\Delta t \cdot P_{t,j}^{\mathrm{dis}}}{e_j}\right] \tag{31}$$

Using the segment-based degradation, we can reconstruct a piecewise linear life loss function d_j^{cyc} that generates the original life loss function in an additive way (Figure 17):

$$d_j^{\mathrm{cyc}} = d_{j-1}^{\mathrm{cyc}} + \Delta e_j^{\mathrm{dis}} \cdot \left(\frac{\Delta\Phi_j}{\Delta\delta_j}\right), \tag{32}$$

where $\Delta e_j^{\mathrm{dis}}$ is the energy discharged from segment *j*.

Figure 17 describes an example of the original life loss function of a LIB as a histogram, its derivative, and the piecewise linear reconstruction of it. The piecewise linear reconstruction is not used in the optimization; it is presented here just to illustrate the concept.

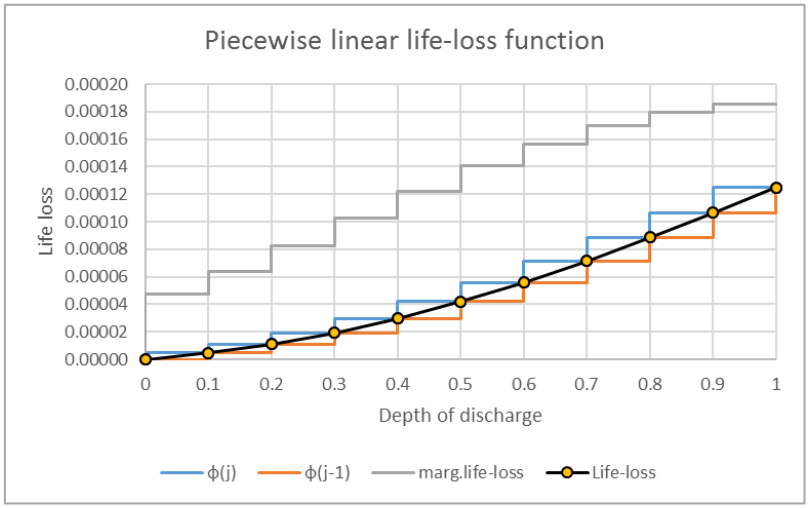

Figure 17: Elements of life loss function.

Finally, the effect of the temperature-to-cycle-life stress factor need to be considered. As the DSF is implemented as a coefficient, it is possible to either add it explicitly in the equations—e.g. to (31)—or to include it implicitly in one of the parameters, i.e., the cycle life of the battery. It would also be beneficial if it would be possible to tune the coefficient

regularly to represent the real historical temperature of the battery. To enable this, a dedicated parameter would be needed for this in the IIP.

3.4.3 Degradation caused by calendar ageing

Normalized calendar ageing as a function of the SOE as well as the associated stress function and a linearized stress function is shown in Figure 18. Linearization of the curve is required in order to be able to use the formulation in a mixed integer programming (MIP) model.

The linearized SOE stress function regarding the calendar life is as follows:

$$S^{\text{cal}}_{\psi,\text{lin}} = q_0 + q \cdot \psi \,, \tag{33}$$

where $q = 1.7$ and $q_0 = 0.3$ for this specific battery type described in Figure 18.

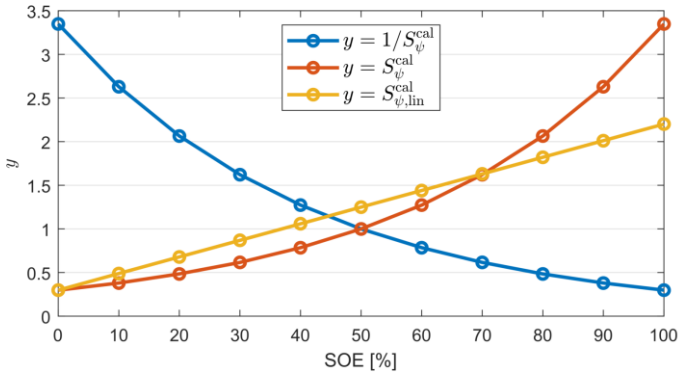

Figure 18: SOE stress factor regarding calendar ageing.

The SOC=50% corresponds to the nominal rate of degradation:

$$\chi = \frac{1}{T_{\text{life}} N_{\text{d-y}} N_{\text{h-d}} N_{\text{ts-h}}} \,, \tag{34}$$

where χ is the calendar-lifetime coefficient, T_{life} is the battery lifetime in years, $N_{\text{d-y}}$ is the number of days per year, $N_{\text{h-d}}$ is the number of hours per day, and $N_{\text{ts-h}}$ is number of time steps per hour. Deviation from the SOE=50% level leads to an accelerated or decelerated rate of degradation according to the DSF value at the corresponding SOE.

Degradation caused by calendar ageing:

$$D^{\text{cal}} = \sum_t s^{\text{cal}}_T \cdot \chi \cdot S^{\text{cal}}_{\psi,\text{lin}}(\psi_t) \tag{35}$$

$$S_{\psi,\mathrm{lin}}^{\mathrm{cal}}(\psi_t) = \left[q_0 + q \cdot \frac{1}{2E} \cdot \left[\Psi(t) + \Psi(t-1) \right] \right], \tag{36}$$

where s_T^{cal} is the coefficient representing the temperature-to-calendar-life stress funtion.

3.4.4 Cost of degradation

The cost of degradation is defined on the basis of lost life using the investment (or replacement) cost, as follows:

$$C_{\mathrm{deg}} = \beta_T \cdot C_{\mathrm{inv}} \cdot \sum_{t}^{T} \left[D_t^{\mathrm{cyc}}(\Delta\delta_t) + D_t^{\mathrm{cal}}(\psi_t) \right], \tag{37}$$

where C_{inv} is the investment cost (or replacement cost) of the battery and β_T is the adaptation coefficient, which can be used to adjust the cost of degradation to achieve the average annual degradation target set by the long-term planning. Long-term planning phase is described in detail in Chapter 4.

3.5 Default parameter mappings

The default parameter mappings for the efficiency and the degradation stress factors are presented in this subsection. These parameter mappings shall be used if there are no BESS-specific parameter mappings available.

3.5.1 Efficiency

The default discharging efficiency characteristics for the battery and the PCS with a power-to-energy (P/E) ratio of 1:1 are shown in Figure 19. The default battery efficiency characteristics were obtained with 98% roundtrip efficiency defined at a rate of C/3. If the battery specification provides a rountrip efficiency $\eta_{\mathrm{spec}}^{\mathrm{rt}}$ at a specified rate I_{spec}, then the discharging/charging efficiency characteristics as a function of current I can be estimated [1] as follows:

$$\eta_{\mathrm{b}}^{\mathrm{ch}} = \eta_{\mathrm{b}}^{\mathrm{dis}} = \sqrt{\frac{1 - a \cdot I}{1 + a \cdot I}} \tag{38}$$

$$a = \frac{1 - \eta_{\mathrm{spec}}^{\mathrm{rt}}}{1 + \eta_{\mathrm{spec}}^{\mathrm{rt}}} \cdot \frac{1}{I_{\mathrm{spec}}}. \tag{39}$$

As the battery efficiency is represented with a constant efficiency in the IIP, the efficiency at the typical operating point shall be used. If the typical operating point is not known in advance, the average value or the value at the nominal power shall be used. The typical operating point can be obtained by performing a simulation with a default efficiency value and by aggregating the resulting power data into segments. An example of the power and energy distribution at 10 % intervals for one-week simulation of the Bulgarian pilot is shown in Figure 20. A good choice for the efficiency would be the value at approximately 85 % of the nominal power, as it represents the typical power level.

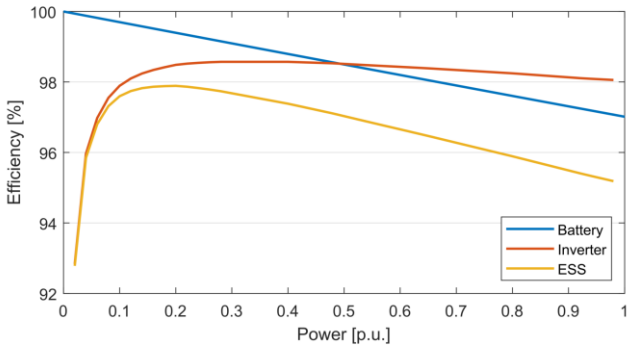

Figure 19: Default battery and inverter efficiency characteristics.

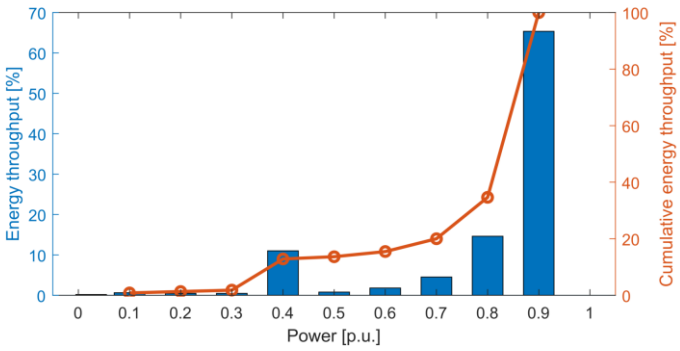

Figure 20: Energy throughput for each power segment. Case study for the Bulgarian pilot.

The default PCS efficiency characteristics were obtained from the specification of a SMA Sunny Tripower STP 60 inverter [10]. The nominal charging and discharging power of the inverter is 60 kW and 75 kW, respectively. There is no transformer included in the system, and therefore, in the efficiency. Consequently, if a transformer is included in the PCS, a slightly lower efficiency shall be used.

The default efficiency mapping can be scaled by using the maximum efficiency provided by the PCS manufacturer. If the technical specification provides a complete efficiency chart, it shall be used instead of the default mapping.

3.5.2 Degradation stress factors

The degradation stress factors are addressed in detail in D6.4 [4]. In general, the adaptation of the degradation stress factor characteristics shall be done specifically for each case, i.e., for each pilot's battery. The stress factor mappings which were shown in Section 3.4.1 shall be used as default mappings.

3.6 Parameters

The input parameters that are needed to run the model are shown in Table 4. Some parameters are used directly in the model or constraints, whereas some parameters are used indirectly to calculate or define other parameters or characteristics of the model. Continuous power ratings shall be used in the model, i.e., peak-power operation is not modelled. The usable energy capacity is impacted by the performance degradation due to ageing. The time-scale of ageing is much longer than the prediction horizon of the optimisation algorithm. Therefore, the energy-capacity parameter can be a constant. However, the parameter needs to be adapted once in a while to the measured or estimated capacity.

Table 4: Parameters that are needed to run the model.

Parameter	Unit	Default	Info	Source
Energy capacity	MWh		Updated regularily	Specification
Discharging power capacity	MW		Continuous rating	Specification
Charging power capacity	MW		Continuous rating	Specification
Battery charging and discharging efficiency	%	98.5%	At typical rate in the application	Calculated based on specification
PCS maximum efficiency	%	98.5%	Maximum value	Specification
Cycle lifetime	FCE		Convert to full cycles equivalent	Specification or warranty terms
Calendar lifetime	years	10 years		Specification or warranty terms
End of life	%	70%	Percentage of the original capacity	Specification or warranty terms
Replacement battery cost	€		Battery system only	Estimation
Cost of degradation tuning parameter		1	Updated regularily	SOH diagnostics
Typical operating temperature	°C	25 °C		Application-specific
Minimum SOE	%	5%		Application-specific
Maximum SOE	%	95%		Application-specific
Power constraint coefficient for charging		0.2		Application-specific
Power constraint coefficient for discharging		0.2		Application-specific

4 Long-term planning

The cost of degradation is used in the operational optimization, as was described in Chapter 3. With this approach, the battery is used only when the available benefits cover also the cost of degradation of the battery. However, this may not always lead to an optimal usage of the battery, as was pointed out in [7]. Moreover, when the investment has been made, the investment cost itself becomes a sunken cost that should not dictate the economic reasoning of the operational phase. Instead, what is of importance is the benefit flow that can be generated by using the battery during its whole lifetime.

The main objective in long-term planning is to define guidelines for the battery use for the planned lifetime. It is assumed here that the use of the battery will be the same each year provided that there aren't any major changes in the environment in which the battery operates. Naturally, changing circumstances call for updated operating procedures.

Maximizing the benefits of using a battery can be carried out as a parametric study in which the battery degradation is used to update parameters. Here we use a simplified inverter model (a constant efficiency) to make the program easier to solve. Then, the objective function does not contain the cost of degradation, but only the costs of electricity purchases. By tightening the constraint on the maximum amount of life lost per year reduces the degradation, reduces the benefits obtained in a year, but prolongs the number of years the battery is able to generate monetary benefits. Here, the discount factor comes into play: the more we appreciate the benefits obtained in the beginning of the planning period, the higher the interest rate should be and the shorter the lifetime of the battery. It is a question of expectations and preferences that dictate the solution.

4.1 Planning procedure

The present value of revenues V_{rev} is calculated by discounting the future revenues R_t at time t with an interest rate i, as follows:

$$V_{\text{rev}} = \sum_{t=0}^{N} \frac{R_t}{(1-i)^t}. \tag{40}$$

The planning process produces the planned battery lifetime, which can be transformed to an average annual degradation rate. When these are fixed, a simple controller can be used to adapt the objective function's cost of degradation level with the help of a β parameter to fulfil the plan.

The planning process is as follows:

- Derive the annual degradation from the planned lifetime T_L for the battery;

$$D_{\text{year}} = \frac{1}{T_L} \tag{41}$$

- Adapt that value to the updating period: If parameter updating takes place seasonally, then divide the yearly value by the number of seasons:

$$D_0 = \frac{1}{N_{\text{period}}} D_{\text{year}} \tag{42}$$

- Update the control parameter based on the measured degradation ΔD_T :

$$\beta_T = \beta_{T-1} + \rho\left(D_0 - \Delta D_T\right) \tag{43}$$

- The beta value is used in the objective function to adapt the cost of degradation so that the measured yearly degradation equals its planned value.

A base value for ρ is 1/ (the length of updating period as a share of year), e.g. 1/0.25 = 4 for seasonal updating. Beta is always bigger than zero. The larger the value, the quicker it attains its final value. The drawback of a large yield is that the value varies more around the final value. The updating can be switched off when the apparent value has been attained. It need not to be updated as long as no major changes either in the environment or in the plan take place. As a final remark, a dedicated parameter needs to be defined in the IIP for tuning the beta coefficient.

4.2 Case example

Long-term planning was applied to the Bulgarian pilot case example[2]. The results are shown in Figure 21. In this particular case, a lifetime of 10 years maximizes the benefits. For interest rates between 7 % and 15 %, the benefit flow is maximized with the battery lifetime of 10 years. With 5 % interest rate, the 20-year result seems marginally more profitable. The lifetime of 10 years translates into a planned annual ΔSOH of 3 %.

[2] The Bulgarian pilot case example is explained in more detail in Section 5.1.

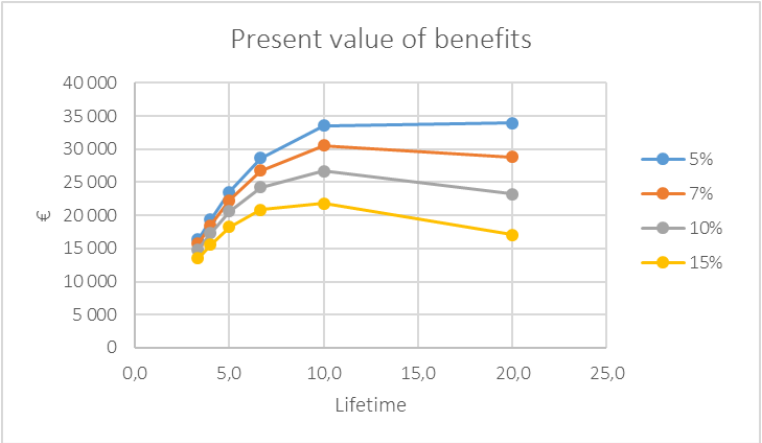

Figure 21: Present value of benefit flows.

The impact of the *ρ* parameter in (43) on the time it takes for the beta parameter to settle is shown in Figure 22. According to the figure, the beta value of 0.4 drives the battery to the right operational range. The beta value is updated seasonally, i.e., four times a year. The original equation is of the form

$$\beta_T = \beta_{T-1} + \rho\left(D_0 - \Delta D_T\right), \tag{44}$$

in which the value for ρ is defined by the length of the beta updating period as a share of a year: 1/0.25 = 4 for seasonal updating. This is the base value for beta. The two other values stand for a sensitivity analysis.

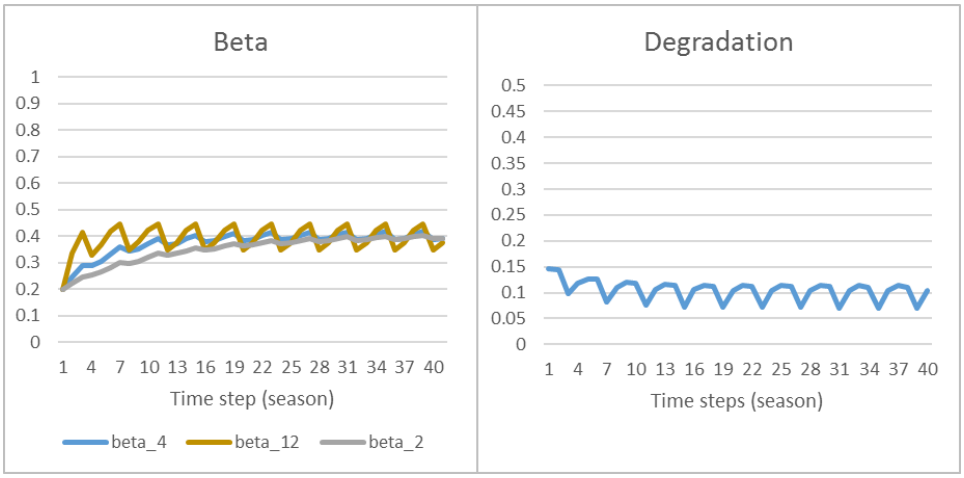

Figure 22: Left panel: Yield parameter (ρ) comparison for a seasonally updated beta-parameter. The common initial value for the beta is 0.2. beta_4 means that beta's value is four. Right panel: Seasonal degradation transformed into a yearly value for the case beta_4.

The beta coefficient is used to make the use of the battery to follow the planned degradation rate. The targeted degradation rate in Figure 22 is 0.1 per year (10 year lifetime) corresponding the results in Figure 21. We have used the same target value for

the degradation in each season, although the optimal use varies by season. This is the prime reason for the cyclic seasonal variation in the beta value (Figure 22).

Figure 23 shows the results of comparing the effect of beta on the use of a battery. It can be seen that with the beta value of 0.4 the battery is used much more aggressively, the cycles being significantly deeper.

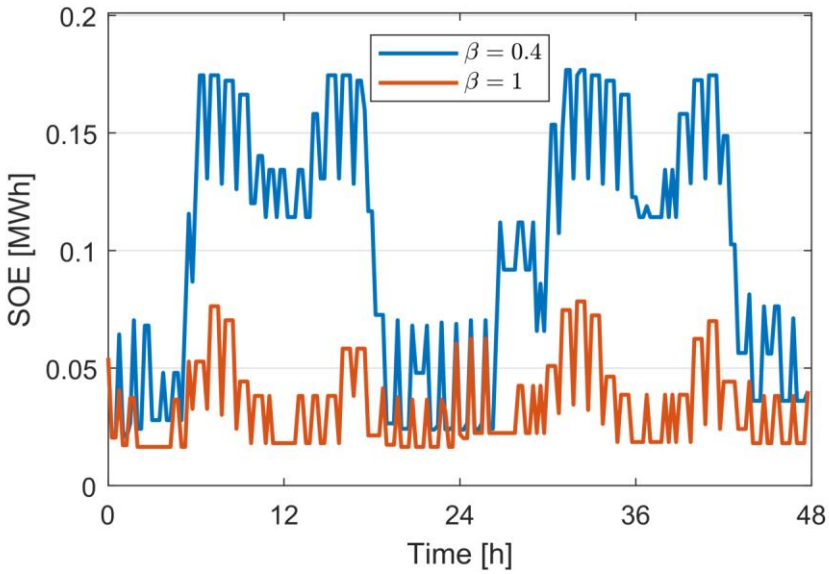

Figure 23: Impact of beta coefficient on the SOE.

5 Implementation and validation

5.1 Case example

The Bulgarian pilot will be used in the examples and case studies. However, in these studies, the electricity price is not constant but varies. The price data was obtained from the Austrian spot market. Therefore, these case studies and examples do not reflect the real situation of the pilot. However, the case studies and examples are used to illustrate the performance and operation of the models and the differences between different modelling methods.

The Bulgarian pilot demonstrates how a centralised battery storage could contribute to the overall energy efficiency of a large energy consumer. At the site of a five-star-hotel Flamingo Grand, a PV installation and a battery storage system have been installed. Currently the PV capacity is 27 kWp, but it is anticipated to be increased significantly in near future. TESVOLT TS HV 70 energy storage system [11] has been installed in the hotel during INVADE project, and therefore, it is used as the battery system in this study. The battery specifications are shown in Table 5. The BESS uses Samsung SDI batteries with NMC technology and SMA inverters. The battery model was parameterized by using the cycle lifetime of 8000 full cycles equivalent (FCE) and the EOL of 70 %.

Table 5: Specification of the battery.

Property	Value
Energy capacity	201 kWh
Power capacity	201 kW
Efficiency	up to 98 %
Cycle life @ 100 % & 1C	6000
Cycle life @ 100 % & C/2	8000
EOL criterion	70 %

The objective function is to minimize the cost of purchased electricity from the grid:

$$\min \sum_t P_g(t) \cdot p_e(t) \Delta t + C_{\text{deg}} \,, \tag{45}$$

where $P_g(t)$ is the grid power at time t, $p_e(t)$ is the corresponding grid electricity price, Δt is the time step, and C_{deg} is the cost of degradation.

The load profile, the PV generation, and the net load profile as well as the electricity price for the two first days of the month of May are shown in Figure 24.

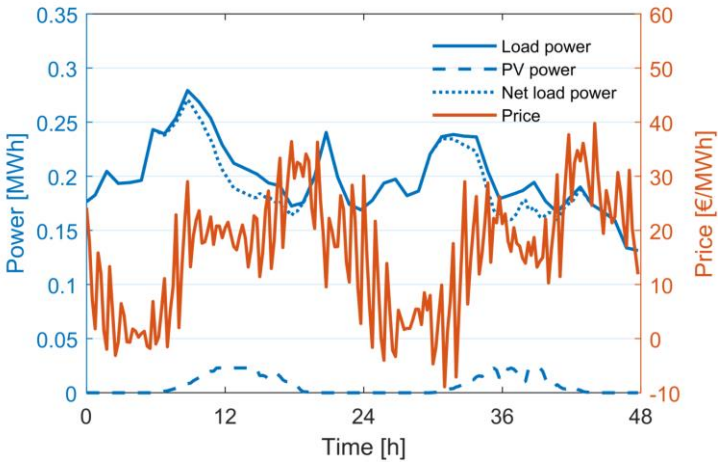

Figure 24: Load profile and electricity price for two days.

5.2 Base model

A battery model with both the cycle ageing and the calendar ageing included as described in Chapter 3 is used as a base model in the simulations. The model also includes the additional power constraints. The beta parameter was set to 0.4 based on the results of the long-term planning presented in Section 4.2.

The net load and the electricity price as well as the resulting optimized BESS charging and discharging power, the grid power, and the SOE are shown in Figure 25. The SOE profile is highly impacted by the electricity price profile, i.e., the battery is charged when the price is low and discharged when the price is the high. Shallow cycles utilize the short-time price volatility, while the deep cycles utilize longer trends in the price profile. The average SOE for the case shown in Figure 25 (two days) is 49 %.

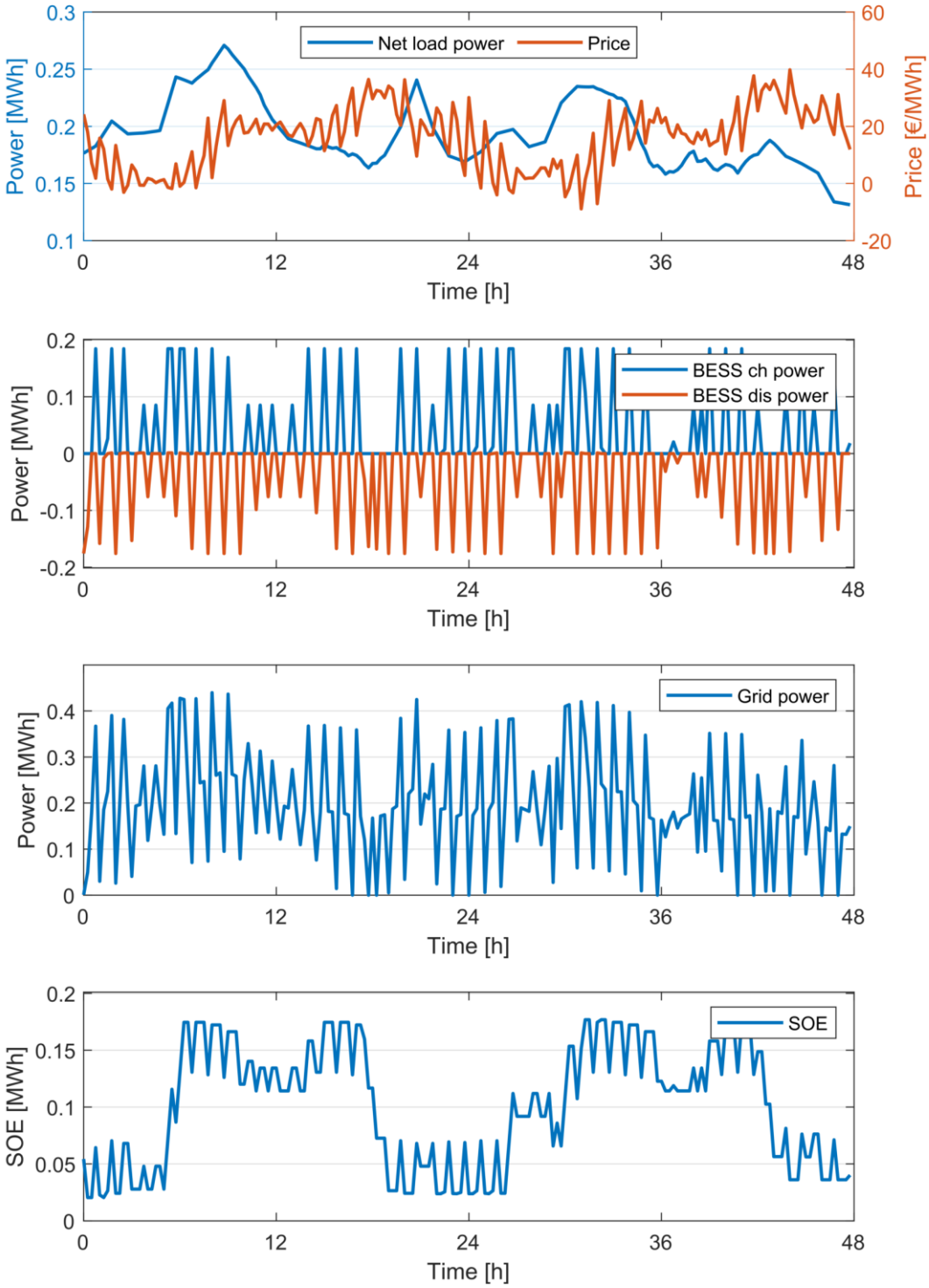

Figure 25: Results of the optimization for the base model. Panels from the top to the bottom: (i) Net load and electricity price. (ii) BESS charging (positive) and discharging (negative) power. (iii) Grid power. (iv) SOE.

5.3 Segment-wise operation

The Bulgarian pilot case example was studied to illustrate the basic operation and the associated cost levels. Here we have defined the minimized cost function using marginal cost of degradation (€/MWh) that is formulated as follows:

$$c_j = \beta_T \left(\frac{C_{\text{inv}}}{E} \right) \cdot \frac{\Delta\Phi\left(\Delta\delta_j\right)}{\Delta\delta_j} = \beta_T \frac{C_{\text{inv}}}{e_j} \cdot \Delta\Phi_j \tag{46}$$

Multiplying this by the energy discharged from the corresponding segment gives the total cost of degradation due to cycling. This formulation gives the same results as the one defined earlier. The difference in these two formulations is that now the degradation in each segment has a specific monetary value representing degradation as a cost of discharging the battery. This cost does not contain the cost of electricity used to charge the battery.

The marginal and average cost of degradation by segment caused by cycle ageing are shown in Figure 26. Using this cost data in the simulation leads to a segment-wise use pattern shown in Figure 27. For a week long period, the discharged energy by segment is shown in Figure 28, which clearly shows how the discharged energy concentrates in the shallow end of the spectrum. The depth of 20 % and 30 % followed by 80 % are the most common cycle depths in the case study, while other cycle depths seem to be marginal.

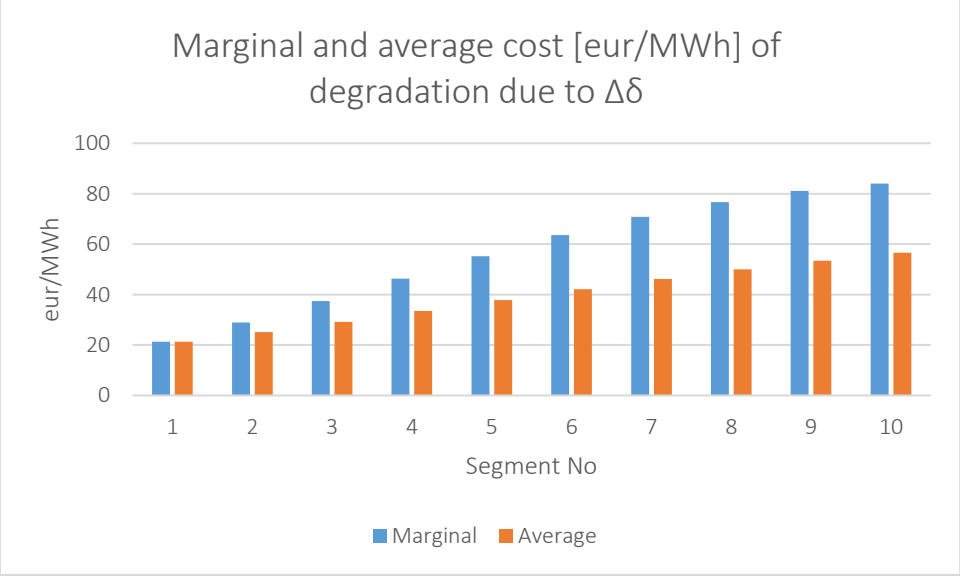

Figure 26: Cycling costs by segment in one pilot case (Δδ=cycle depth).

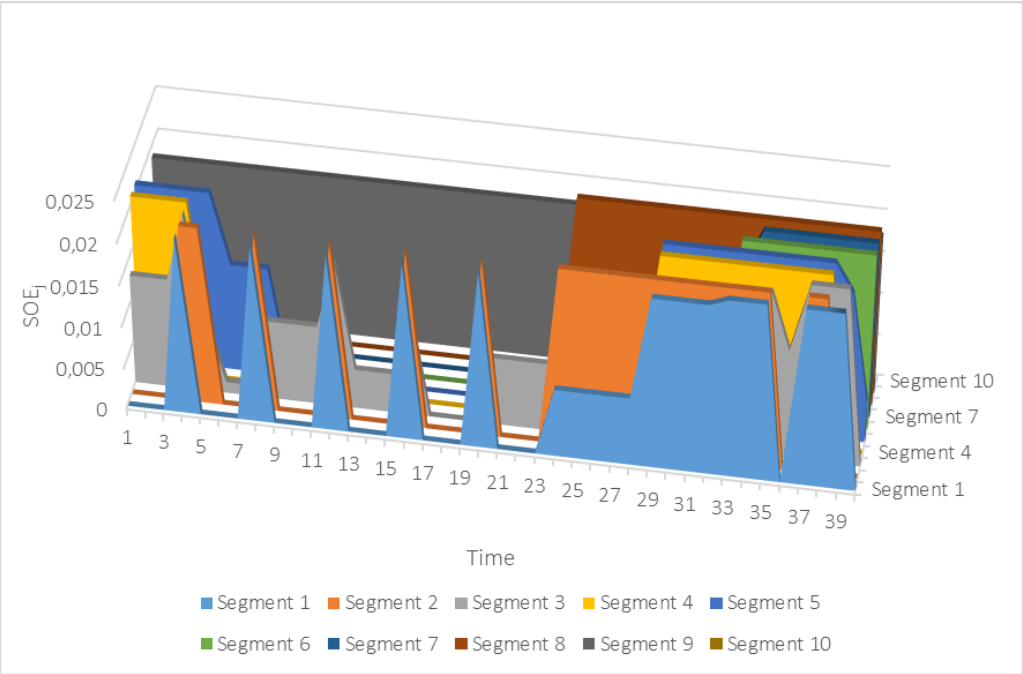

Figure 27: Battery SOE by segment during a 10 hour time span.

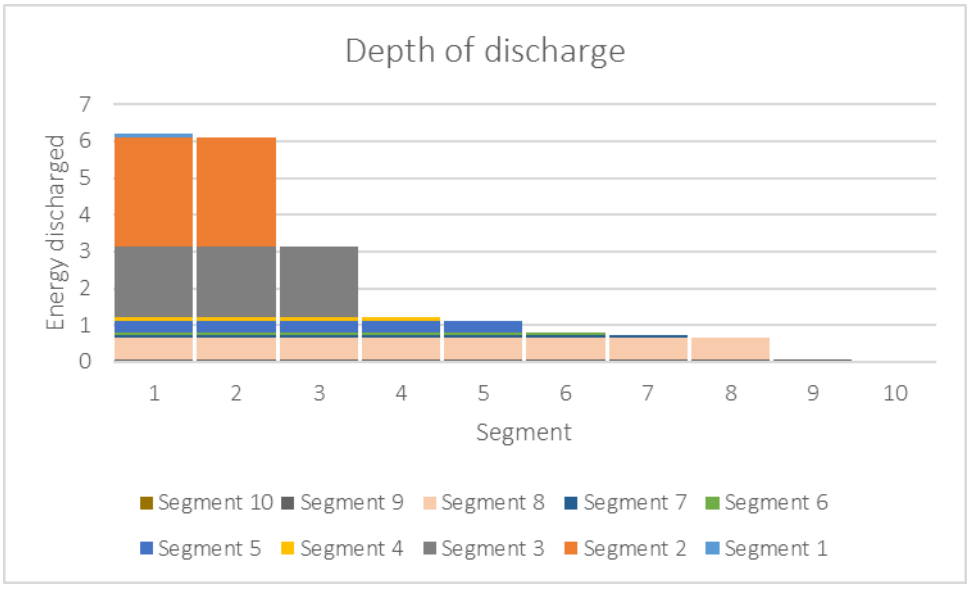

Figure 28: Discharge by segment (vertical) and depth of discharge (horizontal) in a test case.

5.4 Piecewise linear approximation in Pyomo

Pyomo includes several piecewise linear interpolation methods, including the SOS2 method presented in Section 3.3 [12]. Most of these methods require an advanced commercial numerical solver such as Gurobi to work properly. In Pyomo, by default a SOS variable of type 2 is used for interpolating a nonlinear curve after dividing the curve

in different linear segments. However, other methods for this kind of linear approximation can influence the overall optimization.

The inverter efficiency has been considered as nonlinear with respect to the battery charging and discharging power. At each time step, the efficiency is calculated by a piecewise approximation between the defined segments of the efficiency value and battery charging/discharging power. The impact of the piecewise linear approximation methods on the simulation results were studied by using the Bulgarian pilot case example. A simulation period of one month was used. The comparison of the simulation results is presented in Table 6. Only slight deviations in the degradation and the grid electricity price can be observed in the results, with SOS2 being in the middle in both categories. Generally, all methods provide adequate results in this case, and therefore, the selection can be made based on the preference on the solver.

Table 6: Impact of the inverter modelling method on degradation and costs.

Different cases	Label	ΔSOH (%)	Power purchase cost (€)
Standard representation using SOS2 constraints	SOS2	0.20	2967
BigM constraint with binary variables	BIGM_BIN	0.19	2993
BigM constraints with SOS1 variables	BIGM_SOS1	0.19	2983
Convex combination model	CC	0.20	2958
Disaggregated convex combination model	DCC	0.20	2968
Incremental (delta) model	INC	0.21	2964
Logarithmic branching convex solutions	LOG	0.20	2969
Logarithmic disaggregated convex combination model	DLOG	0.22	2963

5.5 Additional discharging and charging power constraints

The additional discharging and charging constraints to avoid reaching the minimum and maximum voltages ensures that the battery is charged slowly enough when approaching fully charged or fully discharged state. The Bulgarian pilot case example was used to study the impact of these additional constraints. The results are shown in Figure 29. It is evident that by using these constraints the actual SOE area where the battery typically operates becomes a little bit narrower, which is expected. Consequently, the cycle depth

of large cycles is typically slightly smaller for the case with the additional constraints. Otherwise, the big picture is similar in both cases, i.e., the constraints do not cause major changes in the operation.

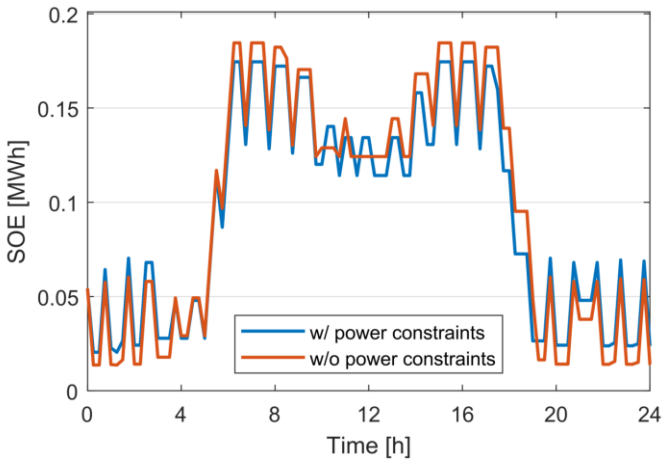

Figure 29: Impact of the additional power constraints to avoid CV charging.

5.6 Cost of degradation

The impact of degradation on the battery use was investigated by defining three versions of the objective function, as follows:

1. No degradation was considered
2. Degradation where only cycle ageing was considered (beta = 0.4)
3. Degradation where both the cycle ageing and the calendar ageing were considered (beta = 0.4)

The example case was simulated for the duration of one week with each of the objective function. The reference power purchase cost for the case with no battery included was 664 €. The actual degradation was calculated similarly for every case. The resulting degradation, power purchase cost, benefit[3], benefit-to-degradation factor (BDF), and expected lifetime are shown in Table 7.

[3] Benefit is defined here as the difference between the reference power purchase cost and the actual power purchase cost.

Table 7: Impact of the degradation model on the battery use.

Case	Degradation (%)	Power purchase cost (€)	Benefit (€)	BDF (€/%)	Lifetime (years)
No degradation (NoDG)	0.63	539	126	200	3.1
Cycle ageing (DG1)	0.21	554	110	519	9.1
Cycle and calendar ageing (DG2)	0.20	556	108	547	9.8

The highest benefit was obtained for the case where no degradation was included in the objective function. However, this case has also the highest degradation (0.63 %), concluding in the lowest BDF and the shortest lifetime. The results for the cases where either only the cycle ageing (DG1) or both the cycle and calendar ageing (DG2) was considered were far better, concluding in the BDF of 519 and 547 €/% and lifetime of 9.1 and 9.8 years, respectively. Cases DG1 and DG2 both show good balance between the degradation and the obtained benefits. In general, the final selection of the degradation model and the value of beta depends on the expected benefit flow and the interest rate, as was discussed in Chapter 4. The above analysis did not take into account the interest rate.

A comparison of the resulting SOE trend for two days duration for the different cases is shown in Figure 30. It is evident that NoDG case uses the battery more aggressively, resulting in higher cycle depths and higher energy throughput. For the cases DG1 and DG2, the overall operation is pretty similar with both methods, but the DG2 results in the average SOE being slightly lower than for DG1. This behaviour was also expected by looking at the SOE DSF shown in Figure 15. Both of these methods can be calibrated to follow the planned degradation rate by tuning the coefficient β.

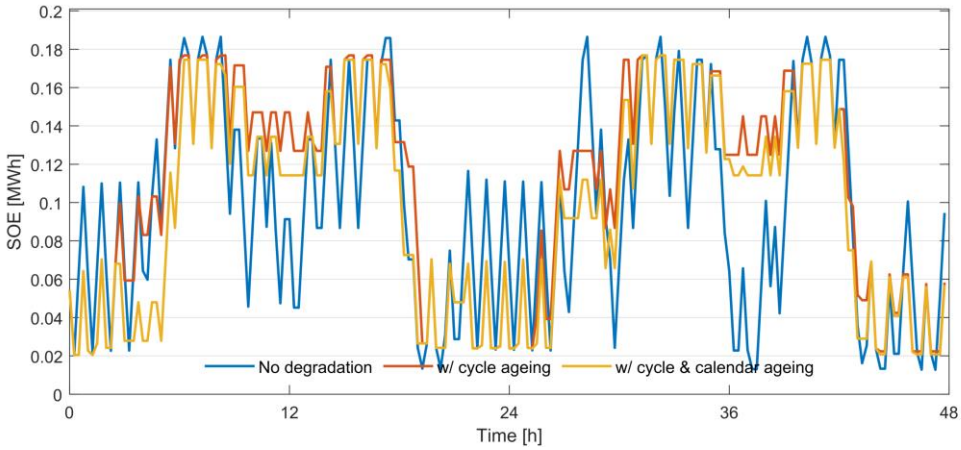

Figure 30: Impact of the cost of degradation modelling methods on the SOE.

References

[1] A. Hentunen, J. Forsström, S. Jenu, S. Tuurala, A. Manninen and S. Bjarghov, “Battery techno-economics tool,” Deliverable D6.2, EU-INVADE, 2018.

[2] S. Ø. Ottesen, P. Olivella-Rosell, P. Lloret, A. Hentunen, P. Crespo del Granado, S. Bjarghov, V. Lakshmanan, J. Aghaei, M. Korpås and H. Farahmand, “Advanced Battery operation and control algorithm,” Deliverable D5.4, EU-INVADE, 2018.

[3] S. Jenu, A. Hentunen, S. Tuurala and A. Manninen, “Simplified state of health diagnostics tool, Deliverable D6.3 EU-INVADE,” 2018.

[4] S. Jenu, S. Tuurala, M. Myllysilta, I. Deviatkin, K. Koponen, A. Manninen and A. Hentunen, “Advanced state of health diagnostics tool, Deliverable D6.4 EU-INVADE,” 2018.

[5] P. Gjerlow, “Pilot specifications,” Deliverable D10.1, EU-INVADE, 2017.

[6] B. Xu, J. Zhao, T. Zheng, E. Litvinov and D. S. Kirschen, “Factoring the Cycle Aging Cost of Batteries Participating in Electricity Markets,” *IEEE Transactions on Power Systems,* 2017.

[7] G. He, Q. Chen, P. Moutis, S. Kar and J. F. Whitacre, “An intertemporal decision framework for electrochemical energy storage management,” *Nature Energy,* vol. 3, pp. 404-412, 2018.

[8] P. T. Moseley and J. Garche, Eds., Electrochemical Energy Storage for Renewable Sources and Grid Balancing, Elsevier, 2014.

[9] M. Skyllas-Kazacos, M. H. Chakrabarti, S. A. Hajimolana, F. S. Mjalli and M. Saleem, “Progress in Flow Battery Research and Development,” *Journal of The Electrochemical Society,* vol. 158, no. 8, pp. R55-R79, 2011.

[10] SMA Solar Technology AG, *Technical Information - Efficiency and Derating: SUNNY BOY / SUNNY BOY STORAGE / SUNNY TRIPOWER / SUNNY MINI CENTRAL v4.3.*

[11] TESVOLT, "TS HV data sheet," [Online]. Available: http://www.tesvolt.com/templates/tesvolt/files/pdf/E.DB.TSHV.ENG-A.20.pdf. [Accessed 21 February 2018].

[12] *Pyomo Documentation, Release 5.1,* 2018.